

d - and p -wave quantum liquid crystal orders in cuprate superconductors, κ -(BEDT-TTF) $_2$ X, and coupled chain Hubbard models: functional-renormalization-group analysis

Rina Tazai¹, Youichi Yamakawa¹, Masahisa Tsuchiizu², and Hiroshi Kontani¹

¹*Department of Physics, Nagoya University, Furo-cho, Nagoya 464-8602, Japan.*

²*Department of Physics, Nara Women's University, Nara 630-8506, Japan.*

(Dated: November 7, 2021)

Unconventional symmetry breaking without spin order, such as the rotational symmetry breaking (=nematic or smectic) orders as well as the spontaneous loop-current orders, have been recently reported in cuprate superconductors and their related materials. They are theoretically represented by non- A_{1g} symmetry breaking in self-energy, which we call the form factor $f_{\mathbf{k},\mathbf{q}}$. In this paper, we analyze typical Hubbard models by applying the renormalization-group (RG) method, and find that various unconventional ordering emerges due to the quantum interference among spin fluctuations. Due to this mechanism, nematic ($\mathbf{q} = \mathbf{0}$) and smectic ($\mathbf{q} \neq \mathbf{0}$) bond orders with d -wave form factor $f_{\mathbf{k},\mathbf{q}} \propto \cos k_x - \cos k_y$ appear in both cuprates and κ -(BEDT-TTF) $_2$ X. The derived bond orders naturally explain the pseudogap behaviors in these compounds. The quantum interference also induces various current orders with odd-parity form factor. For example, we find the emergence of the charge and spin loop-current orders with p -wave form factor in geometrically frustrated Hubbard models. Thus, rich quantum phase transitions with d - and p -wave form factors are driven by the paramagnon interference in many low-dimensional Hubbard models.

I. INTRODUCTION

Various exotic symmetry-breaking, such as violations of the rotational, time-reversal and inversion symmetries, have been discovered in many strongly correlated metals, thanks to the recent progress of experiments. For example, electronic nematic states (=rotational symmetry breaking) without magnetization commonly emerge in Fe-based and cuprate superconductors. These discovered exotic symmetry breaking are generally called the “quantum liquid crystal states”, and they are totally different from conventional local spin/charge density waves (SDW/CDW) studied so far. These exotic orders are “hidden” due to the difficulties in experimental detection, while they are fundamental states of metals because their transition temperatures are frequently higher than conventional SDW/CDW orders. In this article, we investigate the rich variety of exotic orderings in terms of the non- A_{1g} symmetry breaking in self-energy, which is represented as the form factor $f_{\mathbf{k},\mathbf{q}}$, in a unified way.

Figure 1 (a) shows a schematic phase diagram of hole-doped cuprates. Below $T_{\text{CDW}} \sim 200\text{K}$, smectic p -orbital charge-density-wave (p O-CDW) emerges at finite wavevector $\mathbf{q} \approx (\pi/2, 0)$ in many compounds¹⁻⁴. The discovery of this smectic p O-CDW significant progress in theoretical studies. A natural candidate of the order parameter behind the p O-CDW is the d -symmetry bond order (BO) shown in Fig. 1(b), where δt represents the modulation of hopping integrals. Various spin-fluctuation-driven BO mechanisms have been proposed⁵⁻¹³. Also, the pair-density-wave scenarios have been proposed in Refs. 14-18.

Another important unsolved issue is the origin of the pseudogap in the density-of-states (DoS) below T^* . At present, it is an open problem whether the pseudogap is a distinct phase or a continuous crossover. As for the latter

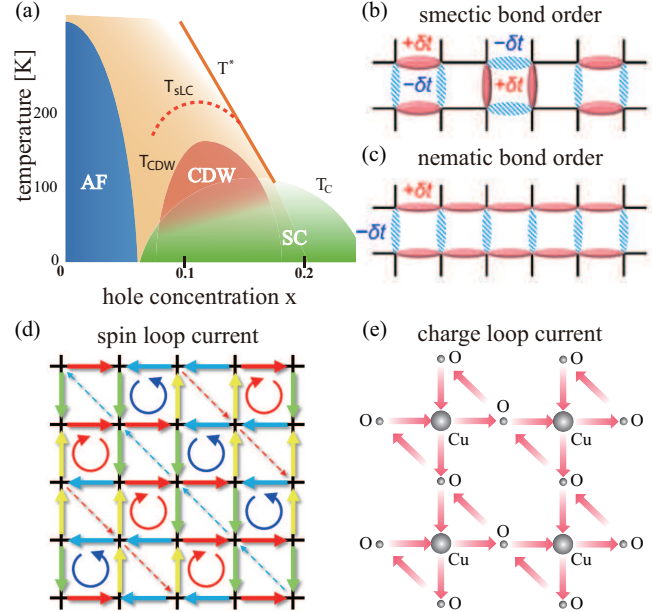


FIG. 1: (a) Schematic phase diagram of hole-doped cuprates. (b) Smectic d -symmetry bond order at $\mathbf{q} = (\pi/2, 0)$ for $T < T_{\text{CDW}}$ and (c) nematic one at $\mathbf{q} = \mathbf{0}$ for $T < T^*$. (d) Spin loop-current order pattern at $\mathbf{q} = (\pi/2, \pi/2)$. (e) Intra-unit-cell charge loop-current proposed in Ref. 19.

case, short-range spin fluctuations at $T \sim T^*$ can induce the pseudogap due to large quasiparticle damping²⁰⁻²². As for the former case, experimental evidence of the phase transition at T^* has been accumulated^{23-27,30}, *e.g.*, the ARPES^{24,25}, magnetic torque^{26,27}, polarized neutron diffraction (PND)^{28,29}, nematic susceptibility³⁰ measurements.

The presence or absence of the time-reversal symme-

try (TRS) in the pseudogap phase has been unsolved for years. We first discuss candidates of TRS preserving order parameter at T^* : Considering the C_4 symmetry breaking below T^{*26} and the enhancement of the nematic susceptibility above T^{*31} , the d -wave nematic ($\mathbf{q} = \mathbf{0}$) order in Fig. 1 (c) would be naturally expected. A similar nematic transition is realized in many Fe-based superconductors^{32–36}. On the other hand, pseudogap is not induced by intra-unit-cell orders. Another candidate of TRS preserving order is the staggered ($\mathbf{q} = \pi/2, \pi/2$) spontaneous spin loop-current (sLC) order shown in Fig. 1(d). The sLC order is “hidden” in that neither internal magnetic field nor charge density modulation is induced, whereas the predicted sLC with finite wavenumber naturally gives the Fermi arc structure and the pseudogap in the DoS.

We also discuss candidates of the TRS broken order parameter at T^* : Figure 1 (e) depicts the intra-unit-cell ($\mathbf{q} = \mathbf{0}$) charge loop current (cLC) order that accompanies the magnetic field proposed by Varma¹⁹. Recently, a number of experimental reports for the cLC order have been accumulated. For instance, in quasi 1D two-leg ladder cuprates, the PND reveal the broken time-reversal symmetry³⁷ and conclude that the cLC appears. The cLCs in the spin disordered phase are also reported in cuprates^{28,29} and iridates³⁸, and their existence is also supported by the optical second harmonic generation (SHG)^{39,40} and Kerr effect⁴¹ measurements.

Theoretically, quantum phase transitions in metals depicted in Figs. 1 (b)-(e) are given by the form factor $\delta t_{i,j}^\sigma$, which corresponds to spontaneous symmetry breaking in self-energy. Here, i, j represent the sites and σ is the spin index. Hereafter, we focus on the exotic nature of the “non-local form factor $i \neq j$ ”. The original hopping integral between sites i and j is modified to $t_{i,j} + \delta t_{i,j}^\sigma$. The Hermite condition leads to the relation $\delta t_{i,j}^\sigma = (\delta t_{j,i}^\sigma)^*$. Here, we set $\delta t_{i,j}^{c(s)} \equiv (\delta t_{i,j}^{\uparrow} + (-)\delta t_{i,j}^{\downarrow})/2$.

For example, the BO is given by a real and even-parity $\delta t_{i,j}^c$, which is shown in Fig. 2 (a)^{5,11,14,42–47}. In contrast, the cLC order is given by a pure imaginary and odd-parity; $\delta t_{i,j}^c = -\delta t_{j,i}^c = \text{imaginary}$ ^{19,48–50}. In this case, $\delta t_{i,j}^c$ represents the fictitious Peierls phase, and the spontaneous cLC is induced as shown in Figs. 2 (b). The cLC order causes the real magnetic field. In contrast, spin current flows if pure imaginary order parameter is odd under space and spin inversions; $\delta t_{i,j}^s = -\delta t_{j,i}^s = \text{imaginary}$. Then, $\delta t_{i,j}^s$ represents the spin-dependent fictitious Peierls phase, and therefore spontaneous sLC order in Figs. 2 (c) is induced^{50–55}.

From the microscopic viewpoint, however, the mechanism of these exotic nonlocal orders is highly nontrivial, since the local ($i = j$) SDW/CDW occurs within the mean-field approximation (MFA). For example, if the Coulomb interaction is local, the induced order is always local within the MFA. One may consider that non-local form factors are realized in extended Hubbard models with non-local Coulomb interaction. However, within the MFA, the realization conditions of nonlocal orders

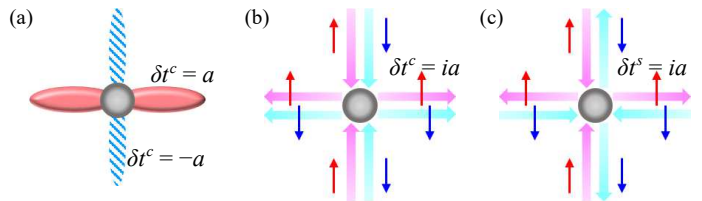


FIG. 2: Form factor $\delta t_{i,j}^{c,s}$ in each nonlocal order: (a) BO ($\delta t_{i,j}^c = \delta t_{j,i}^c = a$), (b) cLC ($\delta t_{i,j}^c = -\delta t_{j,i}^c = ia$), and (c) sLC ($\delta t_{i,j}^s = -\delta t_{j,i}^s = ia$). Here, a is a real quantity.

are severe even in extended U - V - J Hubbard model⁵¹. These facts indicate the importance of non-local effective interaction due to beyond-mean-field many-body effects, called the vertex corrections (VCs). This is the main issue of the present article.

Recently, important roles of the VCs on the nonlocal orders have been revealed step by step. The nematic order in Fe-based superconductors is induced by the Aslamazov-Larkin (AL) VCs^{32–36}, which are significant near the magnetic quantum-critical-point (QCP). The physical meaning of the AL-VCs is the “quantum interference” between different spin fluctuations at \mathbf{Q} and \mathbf{Q}' , which is depicted in Fig. 3. Due to this mechanism, non-local order at $\mathbf{Q} - \mathbf{Q}'$ is established. This mechanism has been applied to many strongly correlated metals to explain various hidden orders^{32–36}. In cuprate superconductors, emergence of the BO and the sLC order has been discussed based on the paramagnon-interference (AL-VC) mechanism^{11,46,47,56}. In addition, other spin-fluctuation-driven mechanisms have been successfully applied^{5–10,12}.

The renormalization group (RG) theory is a very powerful method to study the quantum interference, because huge numbers of parquet-type diagrams are generated by solving the RG differential equation. Although conventional N -patch RG^{57–59} is applicable for a model with simple band dispersion, this constraint is alleviated by combining the RG and the constrained random-phase-approximation (cRPA). Using this RG+cRPA method, we can calculate the general charge (spin) susceptibilities with non-local form factor, $\chi_f^{c(s)}(\mathbf{q})$, by including higher-order VCs. The realized order with form factor f at wavevector \mathbf{q} is determined under the condition of maximizing the function $\chi_f^{c(s)}(\mathbf{q})$.

In this article, we perform the RG analysis of exotic “quantum liquid crystal states” described by non- A_{1g} and non-local form factor in cuprate superconductors, κ -(BEDT-TTF)₂X, and coupled chain Hubbard models. It is clarified that the paramagnon interference mechanism causes rich quantum phase transition with d -wave and p -wave form factors in typical low-dimensional Hubbard models. This paper is organized as follows: In Sect. II, we explain the formalism of the RG method, based on which we derive general charge (spin) channel susceptibility with form factor, $\chi_f^{c(s)}(\mathbf{q})$. We explain how to derive

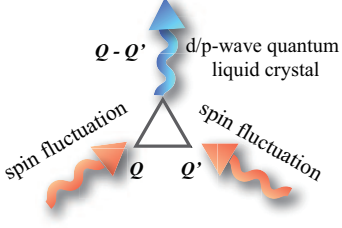


FIG. 3: Interference mechanism due to spin fluctuations. It causes exotic d - and p -wave quantum liquid crystal phases such as nematic/smectic BO, sLC, and cLC orders.

the optimized form factor f . In Sects. III and IV, we discuss the BO order and sLC order formation in cuprate superconductor and κ -(BEDT-TTF)₂X, respectively. In Sect V, we discuss the cLC order induced in the quasi 1D Hubbard model with geometrical fluctuation. The BO, sLC and cLC orders are induced by paramagnon interference mechanism, which is totally dropped in the MFA. The discussions and summary are presented in Sect. VI.

II. RENORMALIZATION GROUP THEORY

“How to treat many-body effects” is one of the long-standing problems in strongly correlated electron systems. Until now, a number of theoretical approaches have been generated^{60–64}, such as dynamical mean-field theory (DMFT) and variational Monte Carlo (VMC) studies. One fundamental approach is perturbation theory based on diagrammatic expansion. However, it is hopeless to consider all possible diagrams, which continue to infinite order. Then, low-order perturbation theory fails to explain strongly correlated systems, such as the Mott transition in cuprates. For long time, the random-phase-approximation (RPA), in which the infinite series of particle-hole loop diagrams are considered, has been used to explain various magnetic transition.

On the other hand, RPA cannot explain recently discovered exotic non-local transitions, since these phenomena originate from mode coupling via spin-, charge-, and orbital-degrees of freedom in nature. Therefore, it is necessary to consider the vertex corrections (VCs) neglected in conventional RPA.

Renormalization group (RG) is a powerful tool to calculate the VCs accurately in an unbiased way. Thanks to the recent theoretical improvement, exotic non-local susceptibilities $\chi_f^{c(s)}(\mathbf{q})$ with form factors $f_{\mathbf{k},\mathbf{q}}$ are analyzed by RG with high accuracy. For instance, in this article, we calculate the non-local susceptibilities in cuprates for nematic/smectic d -symmetry BO as well as p -symmetry sLC and cLC ordered phase. Hereafter, we explain the optimization of form factors within the RG scheme.

A. RG formalism

Here, we explain the RG method based on one-orbital Hubbard models whose interaction part is given by

$$\hat{H}_I = \sum_{\mathbf{k}_i, \sigma_i} \Gamma_{\mathbf{k}_1 \mathbf{k}_2 \mathbf{k}_3 \mathbf{k}_4}^{\sigma_1 \sigma_2 \sigma_3 \sigma_4} c_{\mathbf{k}_1 \sigma_1}^\dagger c_{\mathbf{k}_2 \sigma_2} c_{\mathbf{k}_4 \sigma_3}^\dagger c_{\mathbf{k}_3 \sigma_4}, \quad (1)$$

where $c_{\mathbf{k}\sigma}^\dagger$ is the creation operator of the electron, and $\hat{\Gamma}$ is fully antisymmetrized four-point bare vertex. In the case of on-site Coulomb repulsion U , the non-zero components of $\hat{\Gamma}$ are given as $\Gamma^{\sigma\sigma\bar{\sigma}\bar{\sigma}} = -\Gamma^{\sigma\bar{\sigma}\sigma\bar{\sigma}} = U/4$, so the requirement by the Pauli exclusion principle is satisfied. When the system has SU(2) symmetry in the spin space, the following relation is satisfied,

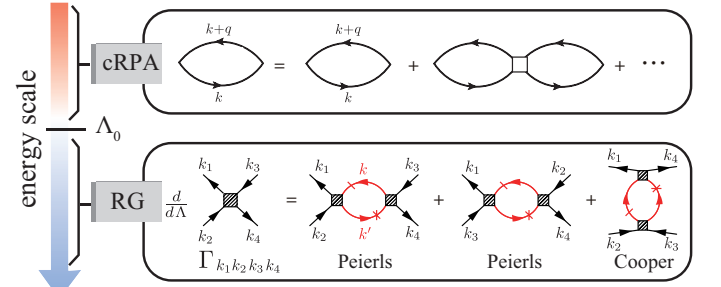
$$\Gamma_{\mathbf{k}_1 \mathbf{k}_2 \mathbf{k}_3 \mathbf{k}_4}^{\sigma\sigma\sigma\sigma} - \Gamma_{\mathbf{k}_1 \mathbf{k}_3 \mathbf{k}_2 \mathbf{k}_4}^{\sigma\sigma\sigma\sigma} = \Gamma_{\mathbf{k}_1 \mathbf{k}_2 \mathbf{k}_3 \mathbf{k}_4}^{\sigma\sigma\bar{\sigma}\bar{\sigma}} - \Gamma_{\mathbf{k}_1 \mathbf{k}_3 \mathbf{k}_2 \mathbf{k}_4}^{\sigma\sigma\bar{\sigma}\bar{\sigma}}. \quad (2)$$

Note that $\Gamma^{\sigma\sigma\sigma\sigma}$ and $\Gamma^{\sigma\sigma\bar{\sigma}\bar{\sigma}}$ stand for four-point vertex function with parallel- (g^{\parallel}) and anti-parallel-spin (g^{\perp}) in g -ology theory^{65–71}. Thus, Eq. (2) is equivalent to the relation $g_1^{\parallel} - g_2^{\parallel} = g_1^{\perp} - g_2^{\perp}$, which we will use in the Sect V. Also, tensor Γ is uniquely decomposed into spin- and charge-channels as

$$\Gamma_{\mathbf{k}_1 \mathbf{k}_2 \mathbf{k}_3 \mathbf{k}_4}^{\sigma\sigma'\rho\rho'} = \frac{1}{2}\Gamma_{\mathbf{k}_1 \mathbf{k}_2 \mathbf{k}_3 \mathbf{k}_4}^s \vec{\sigma}_{\sigma\sigma'} \cdot \vec{\sigma}_{\rho'\rho} + \frac{1}{2}\Gamma_{\mathbf{k}_1 \mathbf{k}_2 \mathbf{k}_3 \mathbf{k}_4}^c \delta_{\sigma\sigma'} \delta_{\rho'\rho}, \quad (3)$$

where $\vec{\sigma}$ is the Pauli matrix vector.

(a) RG+cRPA method



(b) $\frac{d}{d\Lambda} \chi_f^{c(s)}(\mathbf{q}) = \chi_f^{c(s)}(\mathbf{q}) + \frac{d}{d\Lambda} R_{\mathbf{q}\mathbf{k}\mathbf{k}'} = \chi_f^{c(s)}(\mathbf{q}) + R_{\mathbf{q}\mathbf{k}\mathbf{k}'} f_{\mathbf{k},\mathbf{q}}$

optimized form factor $f_{\mathbf{k},\mathbf{q}} = \bullet$

FIG. 4: (a) Diagrammatic explanation of the RG+cRPA method. (b) RG equation of the susceptibility $\chi_f^{c(s)}(\mathbf{q})$ and three-point vertex function $R_{\mathbf{q}\mathbf{k}\mathbf{k}'}$ with the form factor $f_{\mathbf{k},\mathbf{q}}$.

The RG concept is based on the adiabatic condition, in which the energy scale of viewing the electron system gradually changes. For this purpose, the logarithmic energy cutoff is introduced as

$$\Lambda = \Lambda_0 e^{-l} \quad (l \geq 0). \quad (4)$$

Also, the Green function with energy cutoff is defined as

$$G(\mathbf{k}) \equiv (i\epsilon_n - \xi_{\mathbf{k}})^{-1} \Theta(\Lambda - |\xi_{\mathbf{k}}|), \quad (5)$$

where $\xi_{\mathbf{k}}$ is the energy dispersion of the electron, and $k = (\mathbf{k}, \epsilon_n)$ with wavevector \mathbf{k} and fermion Matsubara frequency ϵ_n . Θ is the Heaviside step function reflecting high energy cutoff within the RG framework. Based on the path integral RG formula, fermionic field operators on the energy-shell $\Lambda - d\Lambda < |\xi_{\mathbf{k}}| < \Lambda$ are integrated out. Then, the effective low-energy four-point vertex with $|\xi_{\mathbf{k}}| < \Lambda - d\Lambda$ is obtained. This complex procedure is automatically performed by solving the following differential equation, so-called RG equation. Within the one-loop approximation, it is given by

$$\begin{aligned} \frac{d}{d\Lambda} \Gamma_{\mathbf{k}_1 \mathbf{k}_2 \mathbf{k}_3 \mathbf{k}_4} &= -\frac{T}{N} \sum_{\mathbf{k}, \mathbf{k}', \epsilon_n, \epsilon_m} \frac{d}{d\Lambda} [G(\mathbf{k}, \epsilon_n) G(\mathbf{k}', \epsilon_m)] \\ &\times \left\{ \left[\Gamma_{\mathbf{k}_1 \mathbf{k}_2 \mathbf{k} \mathbf{k}'} \Gamma_{\mathbf{k} \mathbf{k}' \mathbf{k}_3 \mathbf{k}_4} - \Gamma_{\mathbf{k}_1 \mathbf{k}_3 \mathbf{k} \mathbf{k}'} \Gamma_{\mathbf{k} \mathbf{k}' \mathbf{k}_2 \mathbf{k}_4} \right] \delta_{\epsilon_n, \epsilon_m} \right. \\ &\left. + \frac{1}{2} \Gamma_{\mathbf{k}_1 \mathbf{k} \mathbf{k}' \mathbf{k}_4} \Gamma_{\mathbf{k} \mathbf{k}_2 \mathbf{k}_3 \mathbf{k}'} \delta_{\epsilon_n, -\epsilon_m} \right\}. \end{aligned} \quad (6)$$

The first and second terms in the right-hand-side originate from Peierls-channel scattering, while the third one corresponds to the Cooper-channel scattering. Here, we employ the Wick-ordered scheme⁷², in which the cutoff function $\Theta_{<} = \Theta(\Lambda - |\xi_{\mathbf{k}}|)$ is used for the Green function⁴⁵. Thus, the VCs due to the higher-energy processes are included more accurately than the Kadanoff-Wilson scheme for $\Theta_{>} = \Theta(|\xi_{\mathbf{k}}| - \Lambda)$ in Ref. 56.

The renormalization procedure of the four-point vertex function is summarized as follows; (i) At the starting point of $\Lambda = W$ (bandwidth), Γ takes U . (ii) Γ is gradually renormalized toward $\Lambda \rightarrow 0$ by following the RG equation. (iii) Finally, we obtain the effective low-energy Γ including higher-order many-body effects. The final Γ is essentially equal to the one by solving the parquet equation introduced by Abrikosov⁷³.

In general, the best way to consider the many-body processes is applying the RG method (i)-(iii) to the full energy region of electron states by putting $\Lambda_0 = W$. However, in this way, the numerical accuracy is not ensured since it is impossible to fully consider \mathbf{k} - and ϵ_n -dependences of Γ . To improve the numerical accuracy, N -patch RG has been invented^{45,57-59,74}, in which the momentum space of the electron system is divided into finite N -patches. While it is, it fails to explain two-dimensional electron systems, in which k -dependence of band structure plays important roles in nature. Therefore, more reliable RG framework is required to study two-dimensional strongly correlated electron systems such as cuprate superconductors.

B. RG+cRPA with form factor

In an effort to establish more reliable RG to apply two-dimensional electrons, the RG+cRPA method has been recently developed^{56,75-80}. We show the diagrammatic explanation of the RG+cRPA method in Fig. 4 (a). In RG+cRPA method, the energy scale of electron system

is divided into two different region by putting $\Lambda_0 < W$. The higher energy region with $\Lambda_0 < \Lambda < W$ is considered by RPA with fine \mathbf{k} -mesh by dropping the VCs. On the other hand, the lower energy region with $\Lambda < \Lambda_0$ is considered by RG scheme. This hybrid method is based on the intuitive idea that higher-order many-body effects become significant only in low-energy region. Thanks to RG+cRPA, the numerical accuracy of the susceptibilities is drastically improved even in the weak-coupling region.

Here, we consider the important roles of the form factor $f_{\mathbf{k}, \mathbf{q}}$ within the RG+cRPA scheme to explain non-local symmetry breaking such as nematic/smectic d - and p -symmetry orders. The charge- (spin-) channel static susceptibility with form factor is given by

$$\begin{aligned} \chi_{ff'}^{c(s)}(\mathbf{q}) &= \frac{1}{2} \int_0^\beta d\tau \langle O_f^{c(s)}(\mathbf{q}, \tau) O_{f'}^{c(s)}(-\mathbf{q}, 0) \rangle, \quad (7) \\ O_f^{c(s)}(\mathbf{q}) &\equiv \sum_{\mathbf{k}} f_{\mathbf{k}, \mathbf{q}} \left\{ c_{\mathbf{k}_+ \uparrow}^\dagger c_{\mathbf{k}_- \uparrow} + (-) c_{\mathbf{k}_+ \downarrow}^\dagger c_{\mathbf{k}_- \downarrow} \right\}, \quad (8) \end{aligned}$$

where $\mathbf{k}_\pm = \mathbf{k} \pm \mathbf{q}/2$. We denote $\chi_f^{c(s)} \equiv \chi_{ff}^{c(s)}$ hereafter. The RG equation of the charge- (spin-) channel susceptibilities with respect to the form factor $f_{\mathbf{k}, \mathbf{q}}$ are given as

$$\begin{aligned} \frac{d}{d\Lambda} \chi_f^{c(s)}(\mathbf{q}) &= \frac{T}{N} \sum_{\mathbf{k}, \mathbf{k}' \epsilon_n} \frac{d}{d\Lambda} [G(\mathbf{k}, \epsilon_n) G(\mathbf{k}', \epsilon_n)] \delta_{\mathbf{k}', \mathbf{k} + \mathbf{q}} \\ &\times R_{f, \mathbf{q} \mathbf{k} \mathbf{k}'}^{c(s)} R_{f, -\mathbf{q} \mathbf{k}' \mathbf{k}}^{c(s)}, \quad (9) \\ \frac{d}{d\Lambda} R_{f, \mathbf{q} \mathbf{k} \mathbf{k}'}^{c(s)} &= \frac{T}{N} \sum_{\mathbf{p}, \mathbf{p}', \epsilon_n} \frac{d}{d\Lambda} [G(\mathbf{p}, \epsilon_n) G(\mathbf{p}', \epsilon_n)] \delta_{\mathbf{p}', \mathbf{p} + \mathbf{q}} \\ &\times R_{f, \mathbf{q} \mathbf{p} \mathbf{p}'}^{c(s)} \Gamma_{\mathbf{p} \mathbf{p}' \mathbf{k} \mathbf{k}'}^{c(s)}, \quad (10) \end{aligned}$$

where $R_f^{c(s)}$ is the three-point vertex function of charge- (spin-) channel with form factor f , and its initial function is

$$R_{f, \mathbf{q} \mathbf{k} \mathbf{k}'}^{c(s)}(l=0) = f_{(\mathbf{k} + \mathbf{k}')/2, \mathbf{q}} + [\text{cRPA correction}]. \quad (11)$$

The diagrammatic RG flows of $\chi_f^{c(s)}$ and $R^{c(s)}$ are given in Fig. 4 (b). Based on the Lagrange multipliers method, we optimize the form factor $f_{\mathbf{k}, \mathbf{q}}$ so as to maximize the susceptibility. For this purpose, we introduce the Fourier expansion of the form factor as

$$f_{\mathbf{k}, \mathbf{q}} = \sum_{n, m=1}^7 2a_{nm}^{\mathbf{q}} h_n(k_x) h_m(k_y), \quad (12)$$

where $h_n(k) = \{\frac{1}{\sqrt{2}}, \cos k, \cos 2k, \cos 3k, \sin k, \sin 2k, \sin 3k\}$ for $n = 1 - 7$, respectively. The coefficient $a_{nm}^{\mathbf{q}}$ is optimized under the condition $\frac{1}{N} \sum_{\mathbf{k}} |f_{\mathbf{k}, \mathbf{q}}|^2 = 1$ by solving the following eigen equation,

$$\sum_M \chi_{LM}^{c(s)}(\mathbf{q}) a_M^{\mathbf{q}} = \lambda a_L^{\mathbf{q}}, \quad (13)$$

where each index $M \equiv (m, m')$ and $L \equiv (l, l')$ takes $1-7^2$. Here, $\chi_{LM}^{c(s)}$ is the susceptibility with respect to the form factors $f = 2h_m(k_x)h_{m'}(k_y)$ and $f' = 2h_l(k_x)h_{l'}(k_y)$ in Eq. (7). The eigenvalue λ corresponds to the undetermined multiplier in the Lagrange multipliers method. In the following sections, we discuss the exotic non-local orders in cuprates based on the present improved RG+cRPA method with form factor $f_{\mathbf{k},\mathbf{q}}$.

III. d/p -WAVE BOND/SLC ORDER IN CUPRATES

To understand the origin of exotic phase transitions in cuprate superconductors exhibited in Fig. 1, we perform the RG+cRPA analysis by focusing on the importance of the quantum interference (see Fig. 3)^{46,56}. We investigate a three-orbital d - p Hubbard model shown in Fig. 5 (a) for YBCO^{11,42,81}. Its Hamiltonian is given by

$$H_{dp} = \sum_{\mathbf{k},\sigma} \mathbf{c}_{\mathbf{k},\sigma}^\dagger \hat{h}_0(\mathbf{k}) \mathbf{c}_{\mathbf{k},\sigma} + U \sum_{\mathbf{j}} n_{d,\mathbf{j},\uparrow} n_{d,\mathbf{j},\downarrow}, \quad (14)$$

where $\mathbf{c}_{\mathbf{k},\sigma}^\dagger = (d_{\mathbf{k},\sigma}^\dagger, p_{x,\mathbf{k},\sigma}^\dagger, p_{y,\mathbf{k},\sigma}^\dagger)$ is the creation operator for the electron on $d_{x^2-y^2}$, p_x , and p_y orbitals with wavevector \mathbf{k} and spin σ . U is the Coulomb interaction on d -orbital, and $n_{d,\mathbf{j},\sigma} = d_{\mathbf{j},\sigma}^\dagger d_{\mathbf{j},\sigma}$. In the kinetic term $\hat{h}_0(\mathbf{k})$, we introduce the third-nearest d - d hopping -0.1 eV into the first-principles d - p model for La_2CuO_4 ⁸² in order to reproduce YBCO-like Fermi surface (FS) depicted in Fig. 5 (b)¹¹. The electron filling is set to $n = n_d + n_p = 4.9$, corresponding to the hole number $x = 0.1$.

Figure 5 (c) shows the spin susceptibility $\chi^s(\mathbf{q})$ obtained by the RG+cRPA method. The obtained strong spin fluctuations at $\mathbf{Q}_S = (\pi - \delta_s, \pi)$ and $\mathbf{Q}'_S = (\pi, \pi - \delta_s)$ are consistent with the neutron inelastic scattering measurements. As increasing U , $\chi_{\text{max}}^s \equiv \chi^s(\mathbf{Q}_S)$ develops monotonically and diverges at $U = U^{\text{cr}} (\approx 4.5$ eV), as shown in Fig. 5 (d). Thanks to the numerical accuracy of the RG+cRPA method, χ_{max}^s perfectly follows the RPA result for a wide weak-coupling region ($U < 4$ eV).

As seen from Figs. 5 (c) and (d), the cRPA contribution for $\Lambda_0 = 0.5$ eV in the initial value is small but very important for the RG analysis^{78,79}. We verified in Ref. 46 that the numerical results by the RG+cRPA method are *qualitatively* similar to those by conventional patch-RG method, whereas the numerical accuracy is well improved.

Next, we investigate the following B_{1g} -symmetry (d -symmetry) charge susceptibility for p -electrons,

$$\begin{aligned} \chi_d^{p\text{-orb}}(\mathbf{q}) &= \frac{1}{2} \int_0^\beta d\tau \left\langle n_d^{p\text{-orb}}(\mathbf{q}, \tau) n_d^{p\text{-orb}}(-\mathbf{q}, 0) \right\rangle, \\ n_d^{p\text{-orb}}(\mathbf{q}) &\equiv n_x(\mathbf{q}) - n_y(\mathbf{q}) \end{aligned} \quad (15)$$

where $n_{x(y)}(\mathbf{q}) = \sum_{\mathbf{k},\sigma} p_{x(y),\mathbf{k}\sigma}^\dagger p_{x(y),\mathbf{k}+\mathbf{q},\sigma}$ is the p -orbital charge-density-wave (p O-CDW) operator.

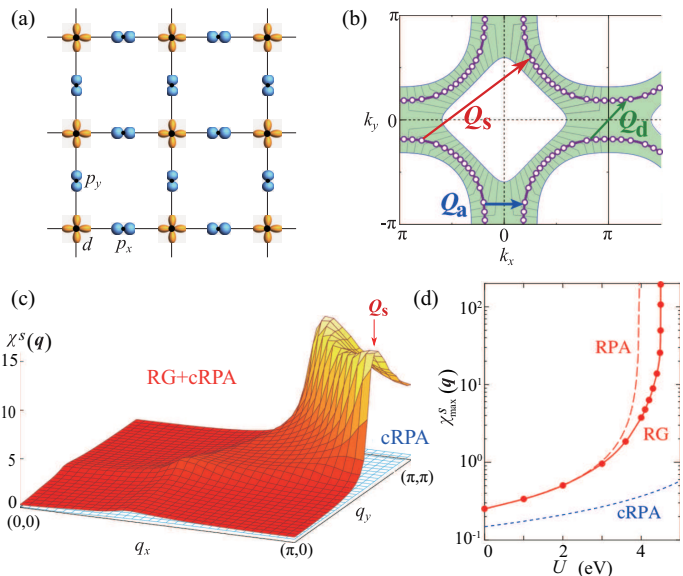


FIG. 5: (a) d - p Hubbard model. (b) Fermi surface (FS) of the present YBCO model. The lower-energy region ($|\xi_{\mathbf{k}}| < \Lambda_0 = 0.5$ eV) is denoted by the shaded area. The N -patch discretization for $N = 64$ is shown, whereas we set $N = 128$ in the present numerical study. (c) Obtained spin susceptibility $\chi^s(\mathbf{q})$. (d) U dependencies of $\chi_{\text{max}}^s \equiv \chi^s(\mathbf{Q}_{rms})$ given by the RG+cRPA method and by the RPA. The initial spin susceptibility given by the cRPA is very small.

Figures 6 (a) and (b) exhibit the obtained $\chi_d^{p\text{-orb}}(\mathbf{q})$ by the RG+cRPA method for $U = 4.32$ eV at $T = 0.1$ eV. The obtained large peaks at $\mathbf{q} = \mathbf{0}$, \mathbf{Q}_a , and \mathbf{Q}_d originate from the VCs, since the RPA result is small and non-singular as seen in Fig. 6 (b). We see that the highest peak locates at $\mathbf{q} = \mathbf{0}$. This is consistent with the experimental uniform nematic transition at T^* ($> T_{\text{CDW}}$)²⁶. The second highest peak locates at $\mathbf{q} = \mathbf{Q}_a$, which naturally explains the CDW phase below T_{CDW} in Fig. 1 (a). Note that the temperature $T = 0.1$ eV is comparable to $T^* \sim 300$ K if the mass-enhancement factor $m^*/m_{\text{band}} \sim 3$ is taken into account.

The enhancement of $\chi_d^{p\text{-orb}}(\mathbf{q})$ in Figs. 6 (a) and (b) is also obtained in the single-orbital Hubbard model, as the enhancement of d -wave bond susceptibility. To explain this fact, we investigate the d -electron charge susceptibility in the d - p Hubbard model with form factor $\chi_f^c(\mathbf{q})$, which is introduced in Eq. (7). We optimize the form factor by following Sect. II. The numerically optimized $f_{\mathbf{k},\mathbf{q}}$ at $\mathbf{q} = \mathbf{0}$ is shown in Fig. 6(c), which has the B_{1g} -symmetry. Its Fourier transformation gives the modulation of the effective hopping integrals, called the $d_{x^2-y^2}$ -wave BO. The \mathbf{k} -dependence of $f_{\mathbf{k},\mathbf{0}}$ in Fig. 6(c) is similar to that of the expectation value of the operator $n_d^{p\text{-orb}}(\mathbf{0})$ on the FS that is proportional to $|u_x(\mathbf{k})|^2 - |u_y(\mathbf{k})|^2$. Here, $|u_{x(y)}(\mathbf{k})|^2$ is the weight of $p_{x(y)}$ orbital at the Fermi momentum \mathbf{k} . Thus, the p O-CDW obtained in the d - p Hubbard model is essentially equivalent to the d -wave BO in the single-orbital Hubbard model.

Next, we discuss the physical picture of the origin of BO obtained by the RG study. To find out the significant quantum process, it is useful to perform the diagrammatic calculations and to compare the obtained results with the RG results. For this purpose, we develop the density-wave (DW) equation method^{33–35,47}. Using this method, we can obtain the most divergent susceptibility with the optimized form factor, by including higher-order VCs. It is clarified that Aslamazov-Larkin (AL) type VCs shown in Fig. 6 (d) are the origin of the enhancement of the p O-CDW susceptibility. Here, red wave lines represent the dynamical spin susceptibility, and the paramagnon interference given by the convolution of χ^s 's, $C_{\mathbf{q}} \equiv \sum_{\mathbf{p}} \chi^s(\mathbf{p}+\mathbf{q})\chi^s(\mathbf{p})$, becomes large $\mathbf{q} \approx \mathbf{Q}_S - \mathbf{Q}_S = \mathbf{0}$ and $\mathbf{q} \approx \mathbf{Q}_S - \mathbf{Q}'_S \approx \mathbf{Q}_d$. This quantum interference gives rise to the BO formation, see Fig. 3. (Note that moderate peak at \mathbf{Q}_d is caused by the single-fluctuation-exchange processes called the Maki-Thompson (MT) VC^{9,10}.)

Both the RG+cRPA method and the DW equation method conclude the emergence of the d -wave BOs at $\mathbf{q} = \mathbf{0}$ and \mathbf{Q}_a in several single-orbital Hubbard models. Thus, the nematic ($\mathbf{q} = \mathbf{0}$) and smectic ($\mathbf{q} \neq \mathbf{0}$) BO formations due to paramagnon interference are expected to be general in many strongly correlated metals. The DW equation method was originally developed to explain the electronic nematic order in Fe-based superconductors^{32,36,83}.

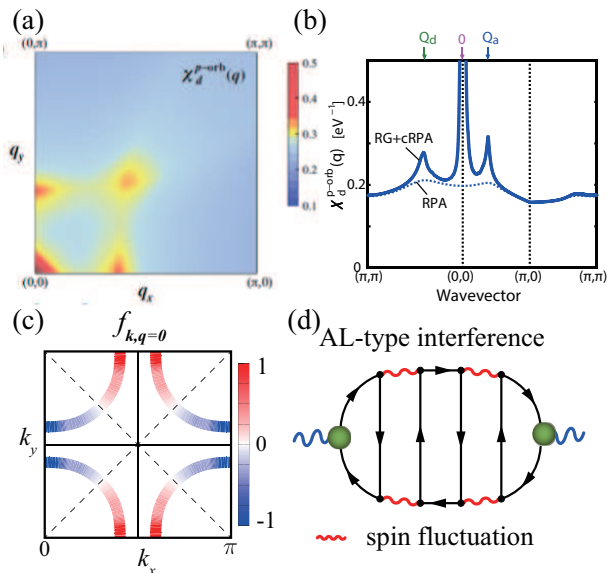


FIG. 6: (a) (b) Obtained p O-CDW susceptibility $\chi_d^{p\text{-orb}}(\mathbf{q})$. The RPA result is also shown for comparison in (b). The obtained peak at $\mathbf{q} = \mathbf{Q}_a$, which corresponds to the nesting vector in Fig. 5 (b), is consistent with experimental CDW wavevector. (c) The optimized form factor $f_{\mathbf{k},\mathbf{q}=\mathbf{0}}$ on the FS, which has the d -symmetry. (d) Example of AL-type vertex corrections that give large p O-CDW susceptibility.

It is noteworthy that the DW equation method also predicts the emergence of the sLC order described by the spin-channel form factor⁸⁴. The predicted transition

temperature T_{sLC} is higher than T_{CDW} . The obtained sLC in real space is shown in Fig. 1 (d). The sLC order is “hidden” in that neither internal magnetic field nor charge density modulation is induced, whereas the predicted sLC naturally explains the pseudogap in the DoS at T^* . It is an important future issue to study the general spin-channel susceptibility with nonlocal form factor based on the RG+cRPA method.

IV. d -WAVE BOND ORDER IN κ -(BEDT-TTF)₂X

The layered organic superconductor κ -(BEDT-TTF)₂X has been attracting great attention as a similar substance to cuprate superconductors. Schematic P - T phase diagram is depicted in Fig. 7 (a)⁸⁵. Under pressure, unconventional superconductivity ($T_c \gtrsim 10\text{K}$) appears next to the antiferro magnetic (AFM) phase^{86,87}. (In X=Cu[N(CN)₂]Br and X=Cu(NCS)₂, metallicity and superconductivity appear even at ambient pressure.) T_{max}^p is the metal-insulator crossover temperature observed in the resistivity. T^* is the pseudogap temperature, below which the NMR relaxation ratio $1/T_1 T$ ^{86,87} and the DoS measured by the STM⁸⁸ exhibit the gap-like behaviors. The nature of the pseudogap and its relation to the superconductivity has been a central mystery in the unconventional metallic states in κ -(BEDT-TTF)₂X.

To study the origin of the pseudogap, we introduce the anisotropic triangular lattice dimer Hubbard model shown in Fig. 7 (b). Each site in the dimer model is composed of the anti-bonding molecular orbital of the BEDT-TTF molecule dimer. This is the simplest effective model for κ -(BEDT-TTF)₂X; $\hat{H} = \hat{H}_0 + \hat{H}_I$ ⁸⁹. The kinetic term is given by $\hat{H}_0 = \sum_{\mathbf{k}\sigma} \xi_{\mathbf{k}} c_{\mathbf{k}\sigma}^\dagger c_{\mathbf{k}\sigma}$ with $\xi_{\mathbf{k}} = 2t(\cos k_x + \cos k_y) + 2t' \cos(k_x + k_y)$. Here, we set the hopping integrals in Fig. 7 (b) as $(t, t') = (-1, -0.5)$. We verified that similar numerical results are obtained for $t'/t = 0.5 \sim 0.8$, which is realized in many κ -(BEDT-TTF) families⁹⁰.

In this dimer Hubbard model, both RPA and FLEX approximation predict the emergence of spin fluctuations at $\mathbf{Q}_S \approx (\pi, \pi)$, consistently with experimental staggered AFM order^{91–94}. These spin fluctuations mediate the $d_{x^2-y^2}$ -wave superconductivity^{91–94}. (Based on more realistic four-site Hubbard models, the d_{xy} -wave state can be obtained in case of weak spin fluctuations at $\mathbf{q} \sim (\pi, 0)$ ⁹⁵.)

In the following numerical study, we set the energy unit $|t| = 1$, and put the temperature $T = 0.05$ and the electron filling $n = 1$ ($\mu = 0.55$). The FS and the band structure are presented in Figs. 7 (c) and (d), respectively. The patch indices (1 ~ 64) are shown on the ellipsoid electron pockets. The total band width is $W \sim 10$ (in unit $|t| = 1$), and $|t|$ corresponds to 0.05eV since $W \sim 0.5\text{eV}$ experimentally^{89,92}.

From now on, we analyze the dimer Hubbard model by applying the RG+cRPA method⁹⁶. The RG+cRPA

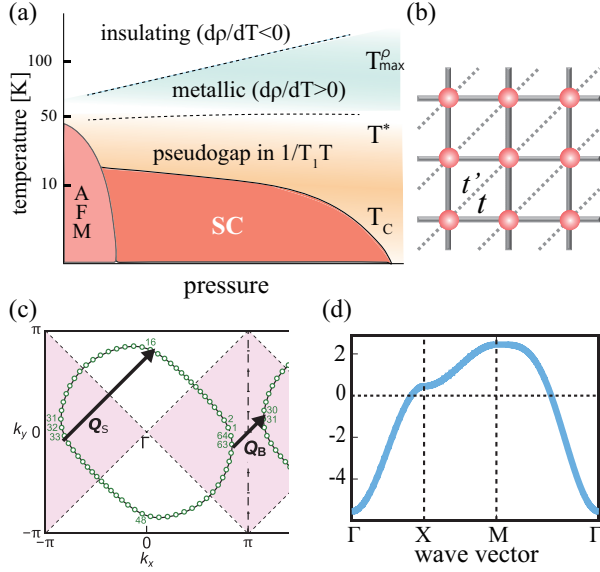


FIG. 7: (a) Schematic P - T phase diagram of κ -(BEDT-TTF) $_2X^{85}$. (b) Anisotropic triangular dimer Hubbard model. (c) FS and (d) band structure of the dimer Hubbard model at half filling with $t'/t = 0.5$.

method is an efficient hybrid method between the RG and the RPA^{46,56,78,80}. Here, we introduce the higher-energy cutoff $\Lambda_0 (= 2)$. The RG flow will stop for $\Lambda_l \lesssim \omega_c$ with $\omega_c = \max\{T, \gamma\}$, where γ ($\propto |\text{Im}\Sigma|$) is the quasi-particle damping rate. Considering large γ in κ -(BEDT-TTF) $_2X$, we introduce the low-energy cutoff $\omega_c = \pi T$ in the RG equation of the four-point vertex Γ in calculating Fig. 4 (a) by following Refs. 46,56.

First, we calculate various spin and charge susceptibilities with the form factor $f_{\mathbf{k},\mathbf{q}}$; $\chi_f^{c(s)}(\mathbf{q})$ introduced in Eq. (7). By analyzing the following from factors $f = 1, \sqrt{2} \sin k_x, \sqrt{2} \sin k_y, \cos k_x - \cos k_y$ and $2 \sin k_x \sin k_y$, we find that the conventional spin susceptibility $\chi^s(\mathbf{q})$ ($= \chi_f^s(\mathbf{q})$ with $f = 1$) and the d -wave bond susceptibility $\chi^{\text{BO}}(\mathbf{q})$ ($= \chi_f^c(\mathbf{q})$ with $f = \cos k_x - \cos k_y$) strongly develop. Other susceptibilities remain small in the present study.

In Fig. 8 (a), we plot \mathbf{q} -dependences of $\chi^{\text{BO}}(\mathbf{q})$ at $U = 3.5$. We reveal the development of $\chi^{\text{BO}}(\mathbf{q})$ at $\mathbf{q} = \mathbf{Q}_B \approx (3\pi/8, 3\pi/8)$ in addition to $\mathbf{q} = (0, 0)$. The obtained strong bond fluctuations originate from the VCs that are dropped in the RPA. (We note that $\chi^{\text{BO}}(\mathbf{q})$ is not enhanced at all in the RPA and FLEX.)

The $\chi^{\text{BO}}(\mathbf{q})$ strongly develops by increasing U . Figure 8 (b) shows the RG flow of the susceptibilities in the case of $U = 3.54$. In this case, the bond susceptibility exceeds the spin one after completing the renormalization. We see that $\chi^s(\mathbf{Q}_S)$ starts to increase in the early stage of the renormalization, by reflecting the major nesting of the FS at $\mathbf{q} = \mathbf{Q}_S$. Next, $\chi^{\text{BO}}(\mathbf{Q}_B)$ starts to increase for $l \gtrsim 3$, and it exceeds $\chi^s(\mathbf{Q}_S)$ at $l \sim 4$. Finally, $\chi^{\text{BO}}(\mathbf{0})$ starts to increase for $l \gtrsim 4$ ($\Lambda_l \lesssim 0.037$), because the

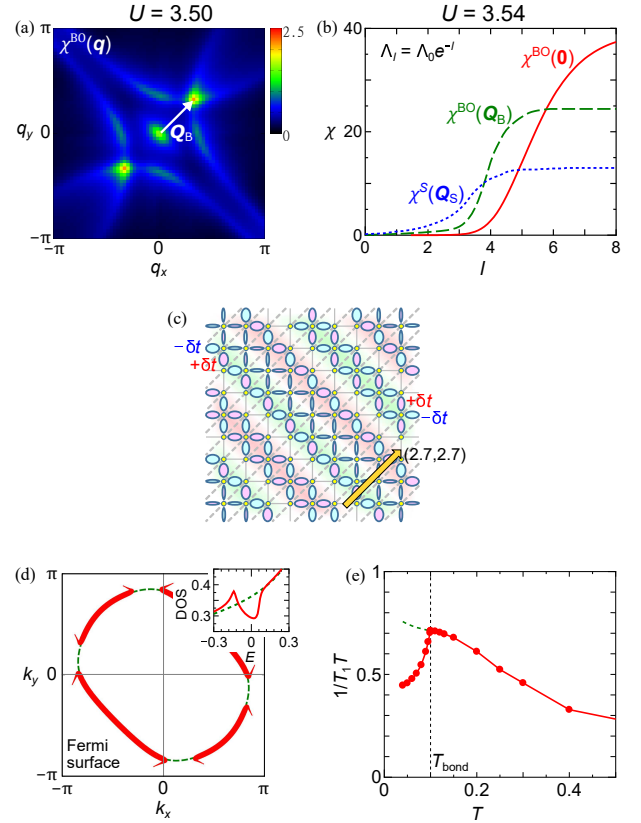


FIG. 8: (a) \mathbf{q} -dependences of $\chi^{\text{BO}}(\mathbf{q})$ obtained by the RG+cRPA method at $U = 3.5$. (b) The RG flow for spin and BO susceptibilities at $U = 3.54$. (c) Schematic BO pattern at $\mathbf{q} = \mathbf{Q}_B$ in real space, where $\lambda \approx (8/3, 8/3)$ is the wavelength vector. (d) Obtained Fermi arc structure in the unfolded zone. The pseudogap in the DoS with $f^{\text{max}} = 0.1$ is shown in the inset. (e) Obtained $1/T_1T$, where T^* is the BO transition temperature.

renormalization of any $\mathbf{q} = \mathbf{0}$ susceptibility occurs only for $\Lambda_l \lesssim T$. All susceptibilities saturate for $l \gtrsim 8$ ($\Lambda_l \lesssim 0.7 \times 10^{-3}$). The final result in Fig. 8 (a) is given at $l \approx 9$. Thus, all $\chi^s(\mathbf{Q}_S)$, $\chi^{\text{BO}}(\mathbf{Q}_B)$ and $\chi^{\text{BO}}(\mathbf{0})$ strongly develop at $U = 3.54$.

Figure 8 (c) shows the schematic d -wave BO pattern at $\mathbf{q} = \mathbf{Q}_B$. Here, each red (blue) ellipse represents the increment (decrement) of the hopping integral δt_μ ($\mu = x, y$) caused by the BO parameters. The opposite sign between the adjacent δt_x and δt_y reflects the d -wave symmetry of the BO. The BO parameter causes the pseudogap in the DoS: Figure 8 (d) shows the Fermi arc structure obtained for $f^{\text{max}} \equiv \max_{\mathbf{k}}\{f_{\mathbf{k},\mathbf{Q}_B}\} = 0.1$. Here, the folded band structure under the BO at $\mathbf{q} = \mathbf{Q}_B$ is “unfolded” into the original Brillouin zone⁹⁷ to make a comparison with ARPES experiment. The resultant pseudogap in the DoS is shown in the inset of Fig. 8 (d), which is consistent with the STM study⁸⁸. The BO leads to significant reduction of the spin fluctuation strength, so the $1/T_1T$ will exhibit kink-like pseudogap behavior. To show that, we calculate the value of $1/T_1T$ in Fig. 8

(e), which is defined as

$$\frac{1}{T_1 T} \propto \sum_{\mathbf{q}, \alpha, \beta} \text{Im} \chi_{\alpha, \beta}^s(\mathbf{q}, \omega) / \omega \Big|_{\omega=0}, \quad (16)$$

where α, β represent the sites in the unit cell under the presence of the BO. We set $f^{\max} = 0.2 \times \tanh(1.74\sqrt{(1-T/T^*)})$ below the BO transition temperature $T^* = 0.1$. (Here, $2f^{\max}(T=0)/T^* = 4$.) The obtained pseudogap behaviors in $1/T_1 T$ and DoS are consistent with phase-transition-like experimental behaviors^{85–87}.

Finally, we discuss that the physical origin of the large ferro-BO ($\mathbf{q} = \mathbf{0}$) and incommensurate-BO ($\mathbf{q} = \mathbf{Q}_B$) instabilities in κ -(BEDT-TTF)₂X model depicted in Fig. 8(a). The obtained large BO instabilities are very similar to those of cuprate and Fe-based superconductors given by the RG+cRPA method and the DW equation analysis. Therefore, the main origin of $\mathbf{q} = \mathbf{0}$ BO and $\mathbf{q} = \mathbf{Q}_B$ BO would be the paramagnon-interference mechanism. On the other hand, $\chi^{\text{BO}}(\mathbf{0})$ is significantly smaller than $\chi^{\text{BO}}(\mathbf{Q}_B)$ in the DW analysis for κ -(BEDT-TTF)₂X model⁹⁶. This result indicates that large peak at $\mathbf{q} = \mathbf{0}$ in the present RG study in Fig. 8(a) originates from the spin and SC fluctuations cooperatively, because the AL process by SC fluctuations can cause the ferro-BO instability as revealed in the previous RG study⁷⁸.

V. TRS BROKEN p -WAVE ORDER: CHARGE LOOP CURRENT

In previous sections, we explained that exotic TRS preserving nonlocal orders are induced by the quantum interference mechanism. The obtained nematic ($\mathbf{q} = \mathbf{0}$) and smectic ($\mathbf{q} \neq \mathbf{0}$) BOs are widely observed not only in cuprates and iridates, but also in Fe-based superconductors. In addition, the sLC naturally explain the pseudogap in the DoS in cuprates.

Also, the emergence of TRS breaking charge-current orders has been actively studied in cuprates and iridates³⁸. Especially, the intra-unit-cell cLC order along the nearest Cu-O-O triangles^{28,29} shown in Fig. 1 (e) has been actively discussed recently. In this Varma cLC order, p orbitals on O atoms contribute to the current order, so extended Hubbard models with O-site and off-site (Cu-O) Coulomb interactions given by U_p and $V_{\text{Cu-O}}$ may have to be analyzed. Within the MFA, however, very huge $V_{\text{Cu-O}}$ is required to explain the cLC. Thus, it is important to find the general mechanism of the cLC order by going beyond the MFA.

To find a general driving force of the cLC order, it is useful to study simple theoretical models accurately using reliable theoretical method. Here, we study the quasi-one-dimensional (q1D) Hubbard model at half-filling ($n = 1$) by applying the RG theory, which becomes more reliable in q1D systems rather than 2D systems. As a result, we reveal that the spin-fluctuation-driven

cLC mechanism, which is expected to be general in low-dimensional Hubbard models with geometrical frustrations.

Below, we study unconventional orders in a geometrically frustrated Hubbard model⁹⁸. The Hamiltonian is $\hat{H} = \hat{H}_0 + \hat{H}_I$, which is schematically shown in Fig. 9 (a). The energy dispersion is simply putted by $\xi_{\mathbf{k}} = -2t \cos k_x - 2t^\perp \{\cos k_y + \cos(k_x + k_y)\} - \mu$ with $t = 1$ and the chemical potential μ . The inter-chain hopping $t^\perp (\ll 1)$ controls the dimensionality; $t^\perp = 0$ corresponds to complete 1D system. The on-site Coulomb interaction is $\hat{H}_I = \sum_i U n_{i\uparrow} n_{i\downarrow}$ where i is the site index. The Fermi surface of the present model is shown in Fig. 9 (b) In the numerical calculation, each left (L) and right (R) Brillouin zone is divided into 24 patches. The logarithmic energy scale for performing the RG is given by $\Lambda_l = \Lambda_0 e^{-l}$ ($0 \leq l \leq l_c$) for $\Lambda_0 = 3$ and $\Lambda_{l_c} = T/100$ ($l_c = 4.6$). We consider the half-filling case and $(t^\perp, T, U) = (0.2, 0.05, 2.01)$ is used.

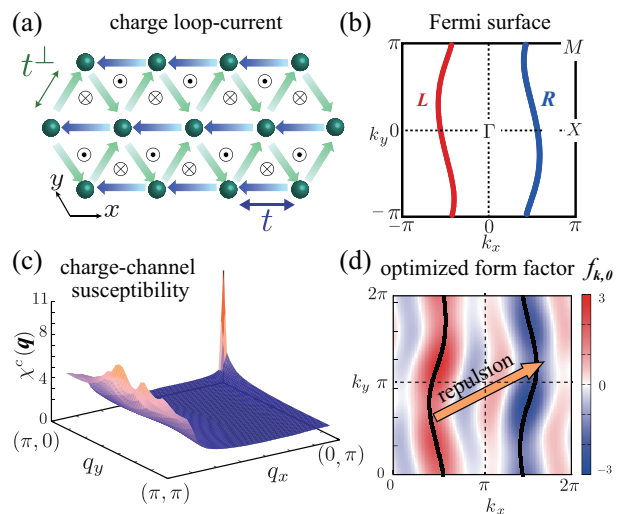


FIG. 9: (a) Present model and obtained charge loop current pattern by RG. (b) FS composed of left (L) and right (R) branches. (c) Obtained charge-channel susceptibility $\chi_f^c(\mathbf{q})$ with the form factor. (d) Optimized charge-channel form factor at $\mathbf{q} = \mathbf{0}$, which corresponds to the uniform charge-loop current.

Based on the RG, we calculate the charge- (spin-) channel susceptibilities with the form factor introduced in Eq. (7). The form factor $f_{\mathbf{k}, \mathbf{q}}$ is optimized unbiasedly to maximize $\chi_f^{c(s)}(\mathbf{q})$ at each \mathbf{q} -point using the Lagrange multipliers method in Sect.II. Figure 9 (c) shows the obtained susceptibility. The strong charge-channel fluctuations develop at $\mathbf{q} = \mathbf{0}$, while the spin fluctuations remain small even at the nesting vector $\mathbf{Q}_S = (\pi, \pi/2)$. Figure 9 (d) shows the \mathbf{k} -dependence of the charge-channel form factor at $\mathbf{q} = \mathbf{0}$. For a fixed k_y , the obtained result shows p -wave symmetry as

$$f_{k_x, k_y, \mathbf{0}} \simeq -f_{-k_x, k_y, \mathbf{0}} \propto \sin k_x + b \sin 3k_x. \quad (17)$$

Then, the real-space order parameter is $\delta t_{ij} = -\delta t_{ji}$,

which leads to the emergence of ferro-type cLC order. Thus, we conclude that the TRS broken p -wave cLC phase is strongly stabilized at $(t, t^\perp) = (0.1, 0.2)$.

From the obtained form factor, we calculate the current from 0-site ($\mathbf{r} = \mathbf{0}$) to i -site ($\mathbf{r} = \mathbf{r}_i$) written by

$$j_i = 2ie \{(t_{i0} + \delta t_{i0})G(-\mathbf{r}_i) - (t_{0i} + \delta t_{0i})G(\mathbf{r}_i)\}, \quad (18)$$

where $-e$ is the charge of an electron. δt_{i0} is the Fourier transformation of charge-channel $f_{\mathbf{k}, \mathbf{q}}$ multiplied by the energy scale Δt . Note that δt_{i0} is pure imaginary and $\delta t_{i0} = -\delta t_{0i}$ holds. The equal-time Green function $G(\mathbf{r}_i)$ in the real space is defined by

$$G(\mathbf{r}_i) = T \sum_{n, \mathbf{k}} \frac{1}{i\epsilon_n - \xi_{\mathbf{k}} - \Delta t f_{\mathbf{k}, \mathbf{0}}} e^{i\mathbf{k}\mathbf{r}_i}. \quad (19)$$

Figures 10 (a) and (b) show the values of the intra- and inter-chain current, respectively. Here, we put $(e, \Delta t) = (1, 0.05)$. We find that the third-nearest-intra-chain form factor is significant to obtain the charge-loop current. In addition, we verified that the macroscopic current is zero due to the cancellation between intra- and inter-chain current. Thus, the present result is consistent with Bloch's theory, which predicts the absence of the macroscopic currents in infinite periodic systems⁹⁹. In Fig. 9 (a), we show the schematic picture of the cLC, which is a magnetic-octupole-toroidal order.

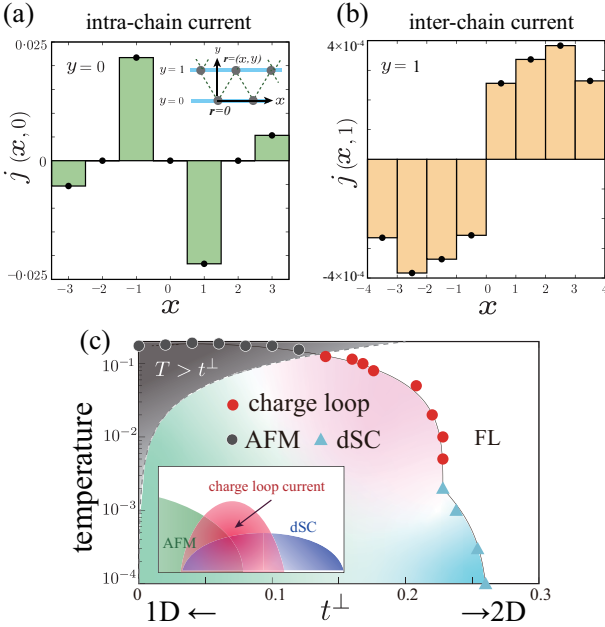


FIG. 10: (a) Obtained intra-chain current $j(x, 0)$ and (b) inter-chain one $j(x, 1)$. (c) Obtained phase diagram. The charge-loop current order appears between anti-ferro magnetic and d -wave superconducting phases.

Figure 10 (c) is obtained phase diagram in the T - t^\perp space. The cLC phase appears around $t^\perp \simeq 0.2$ as an intertwined order between antiferro magnetic and d -wave

superconducting states. Note that the dark shaded area is 1D Mott insulating phase that is beyond the scope of the present study^{67,68}. As a result, the cLC phase is stabilized in the Fermi liquid region around $t^\perp \gg T$.

To understand the origin of the cLC, we analyze the charge- (spin-) channel four-point vertex function based on the g -ology theory defined as

$$g_{aa'}^{c(s)}(\mathbf{q}) \equiv \max_{\mathbf{p} \in a, \mathbf{p}' \in a'} \Gamma_{\mathbf{p}, \mathbf{p}+\mathbf{q}, \mathbf{p}', \mathbf{p}'+\mathbf{q}}^{c(s)} \quad (20)$$

where a, a' are indices of the branch of the FS and takes R ($p_x > 0$) or L ($p_x < 0$) as defined in Fig. 9 (b). Based on the g -ology theory, the $g^{c(s)}$ is classified into backward (g_1), forward (g_2, g_4) and umklapp (g_3) scattering as defined in Fig. 11 (a)⁶⁵⁻⁷¹. There is one-to-one correspondence between $g^{c(s)}$ and $g_{i=1-4}$ as diagrammatically shown in Fig. 11 (b), which is described as

$$g_{RR}^c(\mathbf{0}) \approx 2\pi v_F g_4^\perp, \quad g_{LR}^c(\mathbf{0}) \approx 2\pi v_F (2g_2^\perp - g_1^\perp) \\ g_{RR}^s(\mathbf{Q}_S) \approx -2\pi v_F g_2^\perp, \quad g_{LR}^s(\mathbf{Q}_S) \approx -2\pi v_F g_3^\perp, \quad (21)$$

where $g^{\perp(\parallel)}$ stands for the four-point vertex function with parallel (anti-parallel) spin. To derive Eq. (21), we use the SU(2)-symmetry and anti-commutation relation of the fermion, which leads to

$$g_1^\perp - g_2^\perp = g_1^\parallel - g_2^\parallel. \quad (22)$$

This relation is equivalent to that of Eq. (2). Note that the g_3^\parallel and g_4^\parallel do not affect the physical quantity due to the anti-commutation relation. Thus, all physical quantities are written by using g^\perp without g^\parallel .

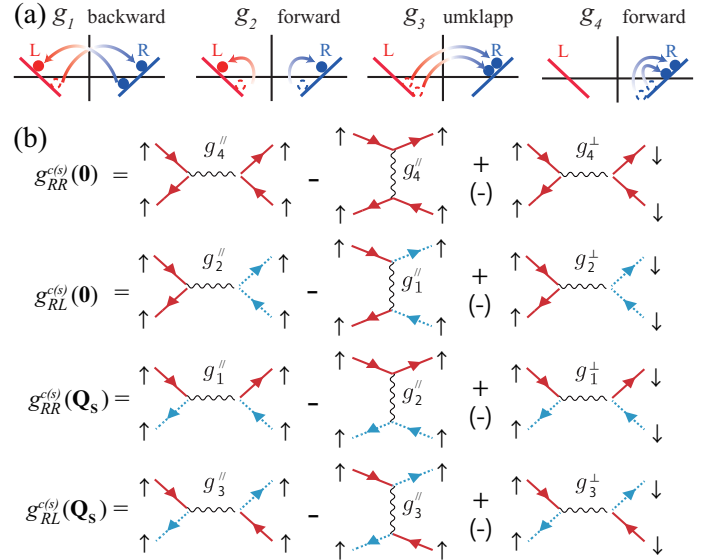


FIG. 11: (a) Definition of the four-point vertex function g_i in the g -ology theory. (b) One-to-one correspondence between $g_{aa'}^{c(s)}(\mathbf{q})$ and $g_i^{\perp(\parallel)}$.

Both $\chi_f^c(\mathbf{0})$ and $\chi_f^s(\mathbf{Q}_S)$ are derived from the RG equations (9)-(11). For a qualitative analysis, we introduce

the following simplified expressions:

$$\chi_f^c(\mathbf{0}) \sim -\{(f_{R,\mathbf{0}})^2 g_{RR}^c(\mathbf{0}) + f_{L,\mathbf{0}} f_{R,\mathbf{0}} g_{LR}^c(\mathbf{0})\} \times (W_{R,R}^+(l^*))^2, \quad (23)$$

$$\chi_f^s(\mathbf{Q}_S) \sim -\{(f_{R,\mathbf{0}})^2 g_{RR}^s(\mathbf{Q}_S) + f_{L,\mathbf{0}} f_{R,\mathbf{0}} g_{LR}^s(\mathbf{Q}_S)\} \times (W_{R,L}^+(l^*))^2, \quad (24)$$

where l^* is an appropriate scaling parameter with $T \ll \Lambda_{l^*} \ll E_F$, and

$$W_{p,p'}^\pm(l) = T \sum_{\mathbf{k}\mathbf{k}'n} G(\mathbf{k}, \epsilon_n) G(\mathbf{k}', \pm\epsilon_n) \Omega_{\mathbf{p}}(\mathbf{k}) \Omega_{\mathbf{p}'}(\mathbf{k}'), \quad (25)$$

where $G(\mathbf{k}, \epsilon_n) = (i\epsilon_n - \xi_{\mathbf{k}})^{-1} \theta(\Lambda_l - |\xi_{\mathbf{k}}|)$, and $\Omega_{\mathbf{p}}(\mathbf{k}) = 1$ (0) only if the momentum \mathbf{k} is inside (outside) of the \mathbf{p} -patch. Figure 12 (a) represents the diagrammatic expression of Eqs. (23) and (24).

In the odd-parity case for $f_{R,\mathbf{0}} = -f_{L,\mathbf{0}}$, the cLC susceptibility is derived from $\chi_f^c(\mathbf{0})$ as

$$\chi^{\text{cLC}}(\mathbf{0}) \propto (f_{R,\mathbf{0}})^2 (-g_4^\perp + 2g_2^\perp - g_1^\perp). \quad (26)$$

Thus, the uniform cLC phase appears due to the coupling constant $-g_4^\perp + 2g_2^\perp - g_1^\perp$. On the other hand, in the even-parity case for $f_{R,\mathbf{0}} = f_{L,\mathbf{0}}$, the AFM susceptibility is derived from $\chi_f^s(\mathbf{Q}_S)$ as

$$\chi^{\text{AFM}}(\mathbf{Q}_S) \propto (f_{R,\mathbf{0}})^2 (g_2^\perp + g_3^\perp). \quad (27)$$

Thus, AFM susceptibility is enlarged due to $g_2^\perp + g_3^\perp$. The classification of general instabilities for $\mathbf{q} = 0, \mathbf{Q}_S$ are summarized in Fig. 12 (b).

Figure 12 (c) shows the obtained RG flow of g_i^\perp . We find that g_4^\perp (g_2^\perp) has large negative (positive) value as l increases, while g_1^\perp and g_3^\perp are quite small. Thus, the strong enhancement of the cLC susceptibility originates from g_2^\perp and g_4^\perp .

To understand the large positive (negative) value of g_2^\perp (g_4^\perp), we consider the classical one-loop RG equation for g_i^\perp , which is given as

$$\begin{aligned} \frac{dg_1^\perp}{dl} &= 2g_1^\perp g_2^\perp I_C + 2g_1^\perp (g_2^\parallel - g_1^\parallel) I_P + 2g_1^\perp g_4^\perp I_L, \\ \frac{dg_2^\perp}{dl} &= (g_2^\perp g_2^\perp + g_1^\perp g_1^\perp) I_C + 2g_4^\perp (g_1^\parallel - g_2^\parallel) I_L \\ &\quad + (g_2^\perp g_2^\perp + g_3^\perp g_3^\perp) I_P, \\ \frac{dg_3^\perp}{dl} &= 2g_3^\perp g_4^\perp I_{C+} + 2g_3^\perp (g_2^\parallel - g_1^\parallel) I_P + 2g_3^\perp g_2^\perp I_P, \\ \frac{dg_4^\perp}{dl} &= (g_4^\perp g_4^\perp + g_3^\perp g_3^\perp) I_{C+} \\ &\quad + 2g_2^\perp (g_1^\parallel - g_2^\parallel) I_L + (g_4^\perp g_4^\perp + g_1^\perp g_1^\perp) I_L. \end{aligned} \quad (28)$$

Their diagrammatic expressions are given in Fig. 13. Here, I_P and I_L denotes the Peierls and Landau channel terms due to the particle-hole loop diagram, and I_C and I_{C+} are the Cooper and Cooper+ channel ones⁶⁵⁻⁷¹. They are expressed as

$$I_{P(L)} \equiv 2\pi\nu_F \cdot dW_{\mathbf{R},\mathbf{L}}^{\pm}(\mathbf{R})/dl, \quad (29)$$

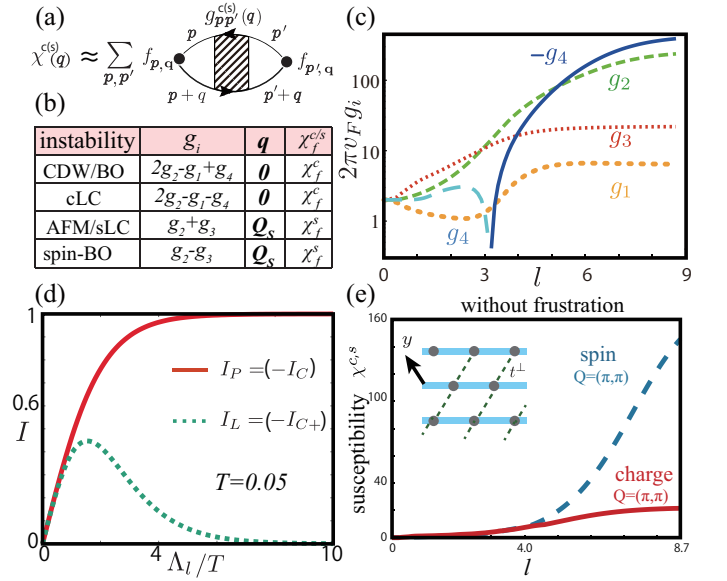


FIG. 12: (a) Diagrammatic expression of susceptibility with form factor. The shaded box is the four-point vertex function by RG. (b) Classification of the charge- and spin-channel instabilities. (c) Obtained RG flow of g_i^\perp . (d) Λ_l -dependence of the $I_P = -I_C$ (red solid line) and $I_L = -I_{C+}$ (green dotted line). (e) Maximum values of $\chi_f^{c(s)}(\mathbf{q})$ without the geometrical frustration.

$$I_{C(C+)} \equiv 2\pi\nu_F \cdot dW_{\mathbf{R},\mathbf{L}}^{\pm}(\mathbf{R})/dl. \quad (30)$$

In the present cLC mechanism, we find that Cooper channel scatterings are negligible since the same cLC phase is obtained even if we neglect I_C and I_{C+} . Thus, the RG equation becomes simpler as

$$\frac{dg_2}{dl} = (g_2^2 + g_3^2)I_P + (-2g_2g_4 + 2g_1g_4)I_L, \quad (31)$$

$$\frac{dg_4}{dl} = (g_4^2 + g_1^2 - 2g_2^2 + 2g_1g_2)I_L, \quad (32)$$

where g_i stands for g_i^\perp for the simplicity and the SU(2) condition is used. Then, g_2 is enhanced by the Peierls-channel term $(g_2^2 + g_3^2)I_P$, while it is suppressed by $-2g_2g_4I_L$ ⁶⁶. On the other hand, g_4 reaches the negative value due to the Landau-channel term $-2g_2^2I_L$. In the 1D region, it is well known that only g_2 is dominant. Therefore, the enhancement of the Landau channel scattering is a key fact to obtain the cLC phase.

Moreover, the Landau-channel scattering becomes important in the presence of geometrical frustration. In fact, finite t^\perp violate the perfect nesting condition, and therefore g_2 is relatively suppressed than the 1D system at $\Lambda_l < t^{\perp 65-70}$. Then, Landau-channel scattering can be enlarged at low-energies ($\Lambda_l < T$) without prohibited by the SDW. Figure 12 (d) exhibits the Λ_l -dependence of $I_{L(P)}$ in the linear dispersion model, which is given by

$$I_P = \tanh(\Lambda_l/2T), \quad (33)$$

$$I_L = (\Lambda_l/2T) \cosh^{-2}(\Lambda_l/2T). \quad (34)$$

Thus, the Landau-channel scattering becomes as important as the Cooper- (Peierls-) scattering in the lower energy region¹⁰⁰. To verify the importance of geometrical frustration, we calculate the $\chi_f^{c(s)}$ by dropping the frustration ($t^\perp = 0$) in Fig. 12 (e). In this case, only spin susceptibility develops, while the charge one is quite small. Thus, the cLC order can overcome the SDW order in the presence of geometrical frustration.

Next, we verify the spin-fluctuation-driven cLC mechanism based on the Fermi liquid theory valid for two-dimensional systems. The important roles of spin fluctuations on the d -wave superconductivity and the non-Fermi liquid-type behaviors (such as $\rho \propto T$ and $R_H \propto T^{-1}$) have been discovered previously¹⁰¹⁻¹⁰⁴. Here, in order to clarify the important role of spin fluctuations on the cLC formation, we solve the DW equation for the charge-channel form factor⁹⁸:

$$\lambda_q f_{\mathbf{k},\mathbf{q}} = \sum_{\mathbf{k}'} f_{\mathbf{k}',\mathbf{q}} L_{\mathbf{k}',\mathbf{q}} \left(-\frac{3}{2} V_{\mathbf{k}-\mathbf{k}'}^s - \frac{1}{2} V_{\mathbf{k}-\mathbf{k}'}^c \right), \quad (35)$$

where λ_q is the eigenvalue and $L_{\mathbf{k},\mathbf{q}} \equiv (n_{\mathbf{k}_-} - n_{\mathbf{k}_+}) / (\xi_{\mathbf{k}_+} - \xi_{\mathbf{k}_-}) > 0$ with Fermi distribution function $n_{\mathbf{k}}$. The interaction $V_{\mathbf{q}}^{c(s)} \equiv -(+)U + U^2 \chi^{c(s)}(\mathbf{q})$ is calculated by the RPA. We find that the cLC solution $f_{\mathbf{k},\mathbf{q}} \propto \sin k_x$ at $\mathbf{q} = \mathbf{0}$ gives the largest eigenvalue due to large $V_{\mathbf{k}-\mathbf{k}'}^s$ at $\mathbf{k} - \mathbf{k}' \approx \pm \mathbf{Q}_S$ ⁹⁸. In solving the DW equation, higher-order fluctuation-exchange processes with respect to $\chi^s(\mathbf{Q}_S)$ are generated. The even (odd)-order processes gives the inter-branch repulsion $g_2 > 0$ (intra-branch attraction $g_4 < 0$), consistently with the g -ology analysis in Fig. 12 (c).

In conclusion, we proposed the microscopic origin of the cLC phase based on the RG theory with optimized form factor. By virtue of this method, the ferro-type cLC order is obtained with high accuracy in a simple frustrated chain Hubbard model. Especially, the geometrical frustration helps the strong enhancement of the forward scattering (g_2 and g_4) via Landau channel scattering. The present study indicates that the cLC can emerge in various metals near the magnetic quantum criticality with geometrical frustration. Thus, the present proposed mechanism can be essential origin of the cLC phases reported in such as cuprates, iridates, and their related materials.

VI. SUMMARY

Exotic symmetry breaking phenomena, such as the nematic/smectic BOs and charge/spin current orders, have

been recently reported in many strongly correlated metals. In this article, we discuss the variety of exotic orderings in terms of the symmetry breaking in self-energy $\delta t_{i,j}^{c,s}$ ($i \neq j$) in a unified way. (Its Fourier transformation gives the form factor $f_{\mathbf{k},\mathbf{q}}^{c,s}$.) Since these exotic order cannot be explained within the mean-field-level approximations, we analyzed beyond-mean-field electron correlations by applying the RG theory.

Based on the RG theory, we found that various types of exotic orders originate from the quantum interference shown in Fig. 3. Due to this mechanism, nematic ($\mathbf{q} = \mathbf{0}$) and smectic ($\mathbf{q} \neq \mathbf{0}$) bond orders with d -wave form factor $f_{\mathbf{k},\mathbf{q}} \propto \cos k_x - \cos k_y$ appear in both cuprates and κ -(BEDT-TTF)₂X. The derived bond order naturally explains the pseudogap behaviors in these compounds. The quantum interference mechanism also causes the sLC order, which naturally explains the pseudogap in the DoS in cuprates. Recently, emergence of the three-dimensional CDW phase under the magnetic field^{105,106} and uniaxial stress¹⁰⁷ has been reported by resonant x-ray measurements in cuprates. It is an important future problem to explain these experiments by using the present fRG method.

In addition, we discussed the emergence of TRS-breaking charge-current orders. The emergence of exotic orders has been discussed by performing precise RG analysis of the q1D Hubbard model. We revealed the spin-fluctuation-driven charge loop-current mechanism, which is expected to be general in low-dimensional Hubbard models with geometrical frustrations. Thus, rich quantum phase transition with d - and p -wave form factors are driven by the paramagnon interference in cuprates and their related materials.

Finally, we comment that the quantum interference (Fig. 3) is significant in f -electron systems with strong spin-orbit interaction. Based on this mechanism, the multipole-fluctuation-pairing mechanism has been discussed in Refs. 108,109, and the fully-gapped s -wave superconductivity without sign reversal in CeCu₂Si₂ is satisfactorily explained. Also, quadrupole and hexadecapole ordering in CeB₆ is also studied¹¹⁰.

Acknowledgments

We are grateful to S. Onari for useful discussions. This work is supported by Grants-in-Aid for Scientific Research (KAKENHI) Research (No. JP20K22328, No. JP20K03858, No. JP19H05825, No. JP18H01175, JP16K05442) from MEXT of Japan.

¹ G. Ghiringhelli, M. L. Tacon, M. Minola, S. Blanco-Canosa, C. Mazzoli, N. B. Brookes, G. M. D. Luca, A. Frano, D. G. Hawthorn, F. He, T. Loew, M. M.

Sala, D. C. Peets, M. Salluzzo, E. Schierle, R. Sutarto, G. A. Sawatzky, E. Weschke, B. Keimer, and L. Braicovich, *Long-Range Incommensurate Charge Fluctu-*

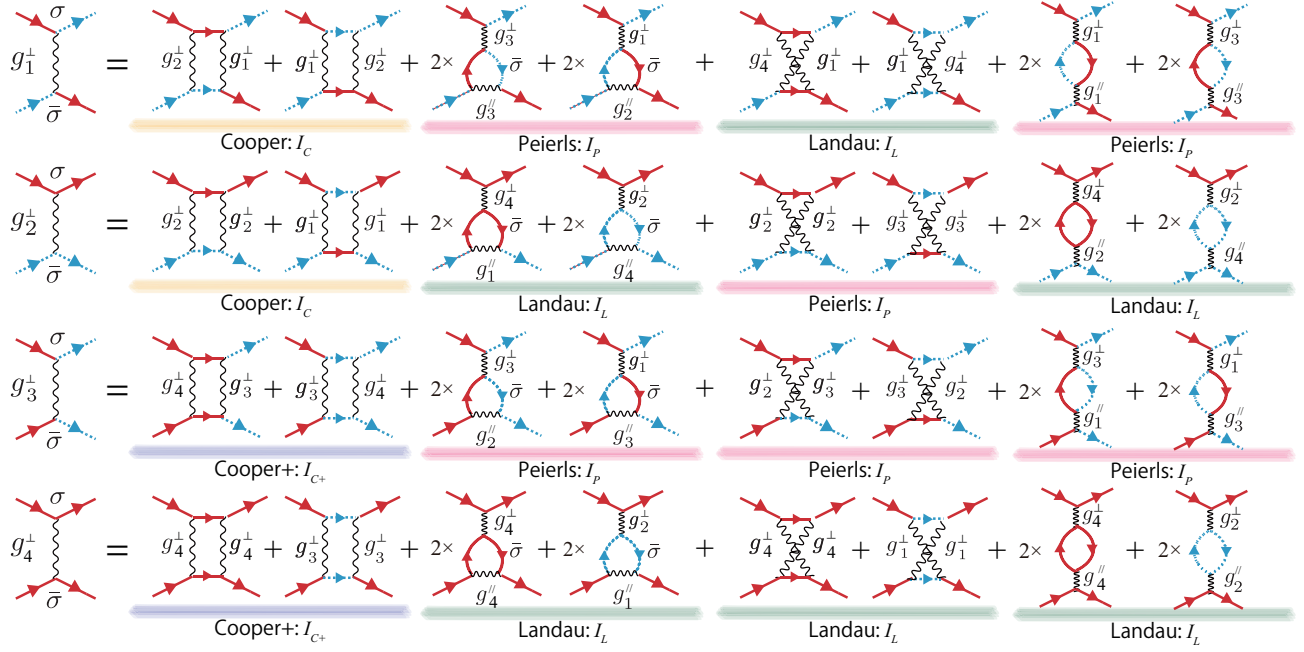


FIG. 13: One-loop RG equation for the four-point vertex function g_i^\perp in g -ology theory.

- ations in $(Y,Nd)Ba_2Cu_3O_{6+x}$, *Science* **337**, 821 (2012).
- ² R. Comin, A. Frano, M. M. Yee, Y. Yoshida, H. Eisaki, E. Schierle, E. Weschke, R. Sutarto, F. He, A. Soumyanarayanan, Y. He, M. L. Tacon, I. S. Elfimov, J. E. Hoffman, G. A. Sawatzky, B. Keimer, and A. Damascelli, *Charge Order Driven by Fermi-Arc Instability in $Bi_2Sr_{2-x}La_xCuO_{6+\delta}$* , *Science* **343**, 390 (2014).
- ³ Y. Kohsaka, T. Hanaguri, M. Azuma, M. Takano, J. C. Davis, and H. Takagi, *Visualization of the emergence of the pseudogap state and the evolution to superconductivity in a lightly hole-doped Mott insulator*, *Nat. Phys.* **8**, 534 (2012).
- ⁴ K. Fujita, M. H. Hamidian, S. D. Edkins, C. K. Kim, Y. Kohsaka, M. Azuma, M. Takano, H. Takagi, H. Eisaki, S. Uchida, A. Allais, M. J. Lawler, E.-A. Kim, S. Sachdev, and J. C. S. Davis, *Direct phase-sensitive identification of a d -form factor density wave in underdoped cuprates*, *Proc. Natl. Acad. Sci. USA* **111**, E3026 (2014).
- ⁵ J. C. S. Davis and D.-H. Lee, *Concepts relating magnetic interactions, intertwined electronic orders, and strongly correlated superconductivity*, *Proc. Natl. Acad. Sci. USA* **110**, 17623 (2013).
- ⁶ M. A. Metlitski and S. Sachdev, *Quantum phase transitions of metals in two spatial dimensions. II. Spin density wave order*, *Phys. Rev. B* **82**, 075128 (2010).
- ⁷ C. Husemann and W. Metzner, *Incommensurate nematic fluctuations in the two-dimensional Hubbard model*, *Phys. Rev. B* **86**, 085113 (2012).
- ⁸ K. B. Efetov, H. Meier, and C. Pépin, *Pseudogap state near a quantum critical point*, *Nat. Phys.* **9**, 442 (2013).
- ⁹ S. Sachdev and R. La Placa, *Bond Order in Two-Dimensional Metals with Antiferromagnetic Exchange Interactions*, *Phys. Rev. Lett.* **111**, 027202 (2013).
- ¹⁰ V. Mishra and M. R. Norman, *Strong coupling critique of spin fluctuation driven charge order in underdoped cuprates*, *Phys. Rev. B* **92**, 060507(R) (2015).
- ¹¹ Y. Yamakawa and H. Kontani, *Spin-Fluctuation-Driven Nematic Charge-Density Wave in Cuprate Superconductors: Impact of Aslamazov-Larkin Vertex Corrections*, *Phys. Rev. Lett.* **114**, 257001 (2015).
- ¹² P. P. Orth, B. Jeevanesan, R. M. Fernandes, and J. Schmalian, *Enhanced nematic fluctuations near an antiferromagnetic Mott insulator and possible application to high- T_c cuprates*, *npj Quantum Materials* **4**, 4 (2019).
- ¹³ H. Yamase, P. Jakubczyk, and W. Metzner, *Phys. Rev. B* **83**, 125121 (2011).
- ¹⁴ E. Berg, E. Fradkin, S. A. Kivelson, and J. M. Tranquada, *Striped superconductors: how spin, charge and superconducting orders intertwine in the cuprates*, *New J. Phys.* **11**, 115004 (2009).
- ¹⁵ E. Fradkin, S. A. Kivelson, and J. M. Tranquada, *Colloquium: Theory of intertwined orders in high temperature superconductors*, *Rev. Mod. Phys.* **87**, 457 (2015).
- ¹⁶ Y. Wang, D. F. Agterberg, and A. Chubukov, *Coexistence of Charge-Density-Wave and Pair-Density-Wave Orders in Underdoped Cuprates*, *Phys. Rev. Lett.* **114**, 197001 (2015).
- ¹⁷ P. A. Lee, *Amperean Pairing and the Pseudogap Phase of Cuprate Superconductors*, *Phys. Rev. X* **4**, 031017 (2014).
- ¹⁸ D. F. Agterberg, J. C. S. Davis, S. D. Edkins, E. Fradkin, D. J. Van Harlingen, S. A. Kivelson, P. A. Lee, L. Radzihovsky, J. M. Tranquada, and Y. Wang, *The Physics of Pair-Density Waves: Cuprate Superconductors and Beyond*, *Annu. Rev. Condens. Matter Phys.* **11**, 231 (2020).
- ¹⁹ C. M. Varma, *Non-Fermi-liquid states and pairing instability of a general model of copper oxide metals*, *Phys. Rev. B* **55**, 14554 (1997).
- ²⁰ D. Sénéchal and A.-M. S. Tremblay, *Hot Spots and Pseudogaps for Hole- and Electron-Doped High-Temperature Superconductors*, *Phys. Rev. Lett.* **92**, 126401 (2004).
- ²¹ B. Kyung, S. S. Kancharla, D. Sénéchal, A.-M. S. Tremblay, M. Civelli, and G. Kotliar, *Pseudogap induced by*

- short-range spin correlations in a doped Mott insulator, Phys. Rev. B **73**, 165114 (2006).
- ²² T. A. Maier, M. S. Jarrell, and D. J. Scalapino, *Understanding high-temperature superconductors with quantum cluster theories*, Physica C: Superconductivity and Its Applications **460-462**, 13 (2007).
- ²³ A. Shekhter, B. J. Ramshaw, R. Liang, W. N. Hardy, D. A. Bonn, F. F. Balakirev, R. D. McDonald, J. B. Betts, S. C. Riggs, and A. Migliori, *Bounding the pseudogap with a line of phase transitions in $YBa_2Cu_3O_{6+\delta}$* , Nature **498**, 75 (2013).
- ²⁴ R.-H. He, M. Hashimoto, H. Karapetyan, J. D. Koralek, J. P. Hinton, J. P. Testaud, V. Nathan, Y. Yoshida, H. Yao, K. Tanaka, W. Meevasana, R. G. Moore, D. H. Lu, S.-K. Mo, M. Ishikado, H. Eisaki, Z. Hussain, T. P. Devereaux, S. A. Kivelson, J. Orenstein, A. Kapitulnik, and Z.-X. Shen, *From a Single-Band Metal to a High-Temperature Superconductor via Two Thermal Phase Transitions*, Science **331**, 1579 (2011).
- ²⁵ S. Nakata, M. Horio, K. Koshiishi, K. Hagiwara, C. Lin, M. Suzuki, S. Ideta, K. Tanaka, D. Song, Y. Yoshida, H. Eisaki, and A. Fujimori, *Nematicity in the pseudogap state of cuprate superconductors revealed by angle-resolved photoemission spectroscopy*, arXiv:1811.10028.
- ²⁶ Y. Sato, S. Kasahara, H. Murayama, Y. Kasahara, E.-G. Moon, T. Nishizaki, T. Loew, J. Porras, B. Keimer, T. Shibauchi, and Y. Matsuda, *Thermodynamic evidence for a nematic phase transition at the onset of the pseudogap in $YBa_2Cu_3O_y$* , Nat. Phys. **13**, 1074 (2017).
- ²⁷ H. Murayama, Y. Sato, R. Kurihara, S. Kasahara, Y. Mizukami, Y. Kasahara, H. Uchiyama, A. Yamamoto, E.-G. Moon, J. Cai, J. Freyermuth, M. Greven, T. Shibauchi, and Y. Matsuda, *Diagonal nematicity in the pseudogap phase of $HgBa_2CuO_{4+\delta}$* , Nat. Commun. **10**, 3282 (2019).
- ²⁸ L. Mangin-Thro, Y. Sidis, A. Wildes, and P. Bourges, *Intra-unit-cell magnetic correlations near optimal doping in $YBa_2Cu_3O_{6.85}$* , Nat. Commun. **6**, 7705 (2015).
- ²⁹ L. Mangin-Thro, Y. Sidis, P. Bourges, S. De Almeida-Didry, F. Giovannelli, and I. Laffez-Monot, *Characterization of the intra-unit-cell magnetic order in $Bi_2Sr_2CaCu_2O_{8+\delta}$* , Phys. Rev. B **89**, 094523 (2014).
- ³⁰ K. Ishida, S. Hosoi, Y. Teramoto, T. Usui, Y. Mizukami, K. Itaka, Y. Matsuda, T. Watanabe, and T. Shibauchi, *Divergent nematic susceptibility near the pseudogap critical point in a cuprate superconductor*, J. Phys. Soc. Jpn. **89**, 064707 (2020).
- ³¹ K. Ishida, M. Tsujii, S. Hosoi, Y. Mizukami, S. Ishida, A. Iyo, H. Eisaki, T. Wolf, K. Grube, H. v Löhneysen, R. M. Fernandes, and T. Shibauchi, *Novel electronic nematicity in heavily hole-doped iron pnictide superconductors*, Proc. Natl. Acad. Sci. USA **117**, 6424 (2020).
- ³² S. Onari and H. Kontani, *Self-consistent Vertex Correction Analysis for Iron-based Superconductors: Mechanism of Coulomb Interaction-Driven Orbital Fluctuations*, Phys. Rev. Lett. **109**, 137001 (2012).
- ³³ S. Onari, Y. Yamakawa, and H. Kontani, *Sign-Reversing Orbital Polarization in the Nematic Phase of FeSe due to the C_2 Symmetry Breaking in the Self-Energy*, Phys. Rev. Lett. **116**, 227001 (2016).
- ³⁴ S. Onari and H. Kontani, *Origin of diverse nematic orders in Fe-based superconductors: 45° rotated nematicity in AFe_2As_2 ($A = Cs, Rb$)*, Phys. Rev. B **100**, 020507(R) (2019).
- ³⁵ S. Onari and H. Kontani, *Hidden antiferromagnetic order in Fe-based superconductor $BaFe_2As_2$ and $NaFeAs$ above T_S* , Phys. Rev. Research **2**, 042005(R) (2020).
- ³⁶ Y. Yamakawa, S. Onari, and H. Kontani, *Nematicity and Magnetism in FeSe and Other Families of Fe-Based Superconductors*, Phys. Rev. X **6**, 021032.
- ³⁷ D. Bounoua, L. Mangin-Thro, J. Jeong, R. Saint-Martin, L. Pinsard-Gaudart, Y. Sidis, and P. Bourges, *Loop currents in two-leg ladder cuprates*, Commun. Phys. **3**, 123 (2020).
- ³⁸ J. Jeong, Y. Sidis, A. Louat, V. Brouet, and P. Bourges, *Time-reversal symmetry breaking hidden order in $Sr_2(Ir,Rh)O_4$* , Nat. Commun. **8**, 15119 (2017).
- ³⁹ L. Zhao, C. A. Belvin, R. Liang, D. A. Bonn, W. N. Hardy, N. P. Armitage, and D. Hsieh, *A global inversion-symmetry-broken phase inside the pseudogap region of $YBa_2Cu_3O_y$* , Nat. Phys. **13**, 250 (2017).
- ⁴⁰ L. Zhao, D. H. Torchinsky, H. Chu, V. Ivanov, R. Lifshitz, R. Flint, T. Qi, G. Cao, and D. Hsieh, *Evidence of an odd-parity hidden order in a spin-orbit coupled correlated iridate*, Nat. Phys. **12**, 32 (2016).
- ⁴¹ V. M. Yakovenko, *Tilted loop currents in cuprate superconductors*, Physica B: Condensed Matter **460**, 159 (2015).
- ⁴² S. Bulut, W. A. Atkinson, and A. P. Kampf, *Spatially modulated electronic nematicity in the three-band model of cuprate superconductors*, Phys. Rev. B **88**, 155132 (2013).
- ⁴³ Y. Wang and A. Chubukov, *Charge-density-wave order with momentum $(2Q, 0)$ and $(0, 2Q)$ within the spin-fermion model: Continuous and discrete symmetry breaking, preemptive composite order, and relation to pseudogap in hole-doped cuprates*, Phys. Rev. B **90**, 035149 (2014).
- ⁴⁴ M. A. Metlitski and S. Sachdev, *Instabilities near the onset of spin density wave order in metals*, New J. Phys. **12**, 105007 (2010).
- ⁴⁵ W. Metzner, M. Salmhofer, C. Honerkamp, V. Meden, and K. Schönhammer, *Functional renormalization group approach to correlated fermion systems*, Rev. Mod. Phys. **84**, 299 (2012).
- ⁴⁶ M. Tsuchiizu, K. Kawaguchi, Y. Yamakawa, and H. Kontani, *Multistage electronic nematic transitions in cuprate superconductors: A functional-renormalization-group analysis*, Phys. Rev. B **97**, 165131 (2018).
- ⁴⁷ K. Kawaguchi, Y. Yamakawa, M. Tsuchiizu, and H. Kontani, *Competing Unconventional Charge-Density-Wave States in Cuprate Superconductors: Spin-Fluctuation-Driven Mechanism*, J. Phys. Soc. Jpn. **86**, 063707 (2017).
- ⁴⁸ I. Affleck and J. B. Marston, *Large- n limit of the Heisenberg-Hubbard model: Implications for high- T_c superconductors*, Phys. Rev. B **37**, 3774(R) (1988).
- ⁴⁹ F. C. Zhang, *Superconducting instability of staggered-flux phase in the $t - J$ model*, Phys. Rev. Lett. **64**, 974 (1990).
- ⁵⁰ H. J. Schulz, *Fermi-surface instabilities of a generalized two-dimensional Hubbard model*, Phys. Rev. B **39**, 2940(R) (1989).
- ⁵¹ A. A. Nersesyan, G. I. Japaridze, and I. G. Kimeridze, *Low-temperature magnetic properties of a two-dimensional spin nematic state*, J. Phys.: Condens. Matter **3**, 3353 (1991).
- ⁵² M. Ozaki, *Broken Symmetry Solutions of the Extended Hubbard Model*, Int. J. Quantum. Chem. **42**, 55 (1992).
- ⁵³ H. Ikeda and Y. Ohashi, *Theory of Unconventional Spin Density Wave: A Possible Mechanism of the Micromagnetism in U-based Heavy Fermion Compounds*, Phys. Rev.

- Lett. **81**, 3723 (1998).
- ⁵⁴ S. Fujimoto, *Spin Nematic State as a Candidate of the Hidden Order Phase of URu₂Si₂*, Phys. Rev. Lett. **106**, 196407 (2011).
- ⁵⁵ S. Zhou, K. Jiang, H. Chen, and Z. Wang, *Correlation Effects and Hidden Spin-Orbit Entangled Electronic Order in Parent and Electron-Doped Iridates Sr₂IrO₄*, Phys. Rev. X **7**, 041018 (2017).
- ⁵⁶ M. Tsuchiizu, Y. Yamakawa, and H. Kontani, *p-orbital density wave with d symmetry in high-T_c cuprate superconductors predicted by renormalization-group + constrained RPA theory*, Phys. Rev. B **93**, 155148 (2016).
- ⁵⁷ D. Zanchi and H. J. Schulz, *Superconducting instabilities of the non-half-filled Hubbard model in two dimensions*, Phys. Rev. B **54**, 9509 (1996).
- ⁵⁸ D. Zanchi and H. J. Schulz, *Weakly correlated electrons on a square lattice: A renormalization group theory*, Europhys. Lett. **44**, 235 (1998).
- ⁵⁹ D. Zanchi and H. J. Schulz, *Weakly correlated electrons on a square lattice: Renormalization-group theory*, Phys. Rev. B **61**, 13609 (2000).
- ⁶⁰ A. Georges, G. Kotliar, W. Krauth, and M. J. Rozenberg, *Dynamical mean-field theory of strongly correlated fermion systems and the limit of infinite dimensions*, Rev. Mod. Phys. **68**, 13 (1996).
- ⁶¹ H. Yokoyama, S. Tamura, and M. Ogata, *Staggered Flux State in Two-Dimensional Hubbard Models*, J. Phys. Soc. Jpn. **85**, 124707 (2016).
- ⁶² C. Weber, T. Giamarchi, and C. M. Varma, *Phase Diagram of a Three-Orbital Model for High-T_c Cuprate Superconductors*, Phys. Rev. Lett. **112**, 117001 (2014).
- ⁶³ T. Schäfer, N. Wentzell, F. Simkovic, Y.-Y. He, C. Hille, M. Klett, C. J. Eckhardt, B. Arzhang, V. Harkov, F.-M. Le Régent, A. Kirsch, Y. Wang, A. J. Kim, E. Kozik, E. A. Stepanov, A. Kauch, S. Andergassen, P. Hansmann, D. Rohe, Y. M. Vilc, J. P. F. LeBlanc, S. Zhang, A.-M. S. Tremblay, M. Ferrero, O. Parcollet, and A. Georges, *Tracking the Footprints of Spin Fluctuations: A Multi-Method, MultiMessenger Study of the Two-Dimensional Hubbard Model*, Phys. Rev. X **11**, 011058 (2021).
- ⁶⁴ J. P. F. LeBlanc, A. E. Antipov, F. Becca, I. W. Bulik, G. K.-L. Chan, C.-M. Chung, Y. Deng, M. Ferrero, T. M. Henderson, C. A. Jiménez-Hoyos, E. Kozik, X.-W. Liu, A. J. Millis, N. V. Prokof'ev, M. Qin, G. E. Scuseria, H. Shi, B. V. Svistunov, L. F. Tocchio, I. S. Tupitsyn, S. R. White, S. Zhang, B.-X. Zheng, Z. Zhu, and E. Gull, *Solutions of the Two-Dimensional Hubbard Model: Benchmarks and Results from a Wide Range of Numerical Algorithms*, Phys. Rev. X **5**, 041041 (2015).
- ⁶⁵ V. J. Emery, R. Bruinsma, and S. Barisić, *Electron-Electron Umklapp Scattering in Organic Superconductors*, Phys. Rev. Lett. **48**, 1039 (1982).
- ⁶⁶ C. Bourbonnais and L. G. Caron, *Renormalization Group Approach to Quasi-One-Dimensional Conductors*, Int. J. Mod. Phys. B **5**, 1033 (1991).
- ⁶⁷ J. Kishine and K. Yonemitsu, *Antiferromagnetic Phase Transition and Crossover to Fermi Liquid Phase in a Weakly Coupled Half-Filled Chain System*, J. Phys. Soc. Jpn. **67**, 2590 (1998).
- ⁶⁸ J. Kishine and K. Yonemitsu, *Dimensional Crossovers and Phase Transitions in Strongly Correlated Low-Dimensional Electron Systems: Renormalization-Group Study*, Int. J. Mod. Phys. B **16**, 711 (2002).
- ⁶⁹ M. Tsuchiizu and Y. Suzumura, *Confinement-deconfinement transition in two coupled chains with umklapp scattering*, Phys. Rev. B **59**, 12326 (1999).
- ⁷⁰ K. Kajiwara, M. Tsuchiizu, Y. Suzumura, and C. Bourbonnais, *Mechanism for the Singlet to Triplet Superconductivity Crossover in Quasi-One-Dimensional Organic Conductors*, J. Phys. Soc. Jpn. **78**, 104702 (2009).
- ⁷¹ J. Sólyom, *The Fermi gas model of one-dimensional conductors*, Adv. Phys. **28**, 201 (1979).
- ⁷² M. Salmhofer, *Continuous Renormalization for Fermions and Fermi Liquid Theory*, Comm. Math. Phys. **194**, 249 (1998).
- ⁷³ A. A. Abrikosov, *Electron scattering on magnetic impurities in metals and anomalous resistivity effects*, Physique Physique Fizika **2**, 5 (1965).
- ⁷⁴ C. J. Halboth and W. Metzner, *d-Wave Superconductivity and Pomeranchuk Instability in the Two-Dimensional Hubbard Model*, Phys. Rev. Lett. **85**, 5162 (2000).
- ⁷⁵ K. Penc and F. Mila, *Charge gap in the one-dimensional dimerized Hubbard model at quarter-filling*, Phys. Rev. B **50**, 11429 (1994).
- ⁷⁶ M. Tsuchiizu and A. Furusaki, *Phase Diagram of the One-Dimensional Extended Hubbard Model at Half Filling*, Phys. Rev. Lett. **88**, 056402 (2002).
- ⁷⁷ M. Tsuchiizu and A. Furusaki, *Ground-state phase diagram of the one-dimensional half-filled extended Hubbard model*, Phys. Rev. B **69**, 035103 (2004).
- ⁷⁸ M. Tsuchiizu, Y. Ohno, S. Onari, and H. Kontani, *Orbital Nematic Instability in the Two-Orbital Hubbard Model: Renormalization-Group + Constrained RPA Analysis*, Phys. Rev. Lett. **111**, 057003 (2013).
- ⁷⁹ M. Tsuchiizu, Y. Yamakawa, S. Onari, Y. Ohno, and H. Kontani, *Spin-triplet superconductivity in Sr₂RuO₄ due to orbital and spin fluctuations: Analyses by two-dimensional renormalization group theory and self-consistent vertex-correction method*, Phys. Rev. B **91**, 155103 (2015).
- ⁸⁰ R. Tazai, Y. Yamakawa, M. Tsuchiizu, and H. Kontani, *Functional renormalization group study of orbital fluctuation mediated superconductivity: Impact of the electron-boson coupling vertex corrections*, Phys. Rev. B **94**, 115155 (2016).
- ⁸¹ A. Thomson and S. Sachdev, *Charge ordering in three-band models of the cuprates*, Phys. Rev. B **91**, 115142 (2015).
- ⁸² P. Hansmann, N. Parragh, A. Toschi, G. Sangiovanni, and K. Held, *Importance of d-p Coulomb interaction for high T_C cuprates and other oxides*, New J. Phys. **16**, 033009 (2014).
- ⁸³ H. Kontani and Y. Yamakawa, *Linear Response Theory for Shear Modulus C₆₆ and Raman Quadrupole Susceptibility: Evidence for Nematic Orbital Fluctuations in Fe-based Superconductors*, Phys. Rev. Lett. **113**, 047001 (2014).
- ⁸⁴ H. Kontani, Y. Yamakawa, R. Tazai, and S. Onari, *Odd-parity spin-loop-current order mediated by transverse spin fluctuations in cuprates and related electron systems*, Phys. Rev. Research **3**, 013127 (2021).
- ⁸⁵ M. R. Beaumont, P. Hemme, Y. Gallais, A. Sacuto, K. Jacob, L. Valade, D. de Caro, C. Faulmann, and M. Cazayous, *Possible observation of the signature of the bad metal phase and its crossover to a Fermi liquid in κ-(BEDT-TTF)₂Cu(NCS)₂ bulk and nanoparticles by Raman scattering*, J. Phys.: Condens. Matter **33**, 125403 (2021).
- ⁸⁶ K. Kanoda, *Electron correlation, metal-insulator transi-*

- tion and superconductivity in quasi-2D organic systems, $(ET)_2X$, Physica C: Superconductivity **282-287**, 299 (1997).
- ⁸⁷ K. Kanoda and R. Kato, *Mott Physics in Organic Conductors with Triangular Lattices*, Annu. Rev. Condens. Matter Phys. **2**, 167 (2011).
- ⁸⁸ T. Arai, K. Ichimura, K. Nomura, S. Takasaki, J. Yamada, S. Nakatsuji, and H. Anzai, *Superconducting and normal-state gaps in κ -(BEDT-TTF) $_2$ Cu(NCS) $_2$ studied by STM spectroscopy*, Solid State Commun. **116**, 679 (2000).
- ⁸⁹ H. Kino and H. Fukuyama, *Phase Diagram of Two-Dimensional Organic Conductors: (BEDT-TTF) $_2$ X*, J. Phys. Soc. Jpn. **65**, 2158 (1996), and references therein.
- ⁹⁰ B. J. Powell and R. H. McKenzie, *Quantum frustration in organic Mott insulators: from spin liquids to unconventional superconductors*, Rep. Prog. Phys. **74**, 056501 (2011).
- ⁹¹ J. Schmalian, *Pairing due to Spin Fluctuations in Layered Organic Superconductors*, Phys. Rev. Lett. **81**, 4232 (1998).
- ⁹² H. Kino and H. Kontani, *Phase Diagram of Superconductivity on the Anisotropic Triangular Lattice Hubbard Model: An Effective Model of κ -(BEDT-TTF) Salte*, J. Phys. Soc. Jpn. **67**, 3691 (1998).
- ⁹³ H. Kondo and T. Moriya, *Spin Fluctuation-Induced Superconductivity in Organic Compounds*, J. Phys. Soc. Jpn. **67**, 3695 (1998).
- ⁹⁴ H. Kontani and H. Kino, *Theory of the Hall coefficient and resistivity for the layered organic superconductors κ -(BEDT-TTF) $_2$ X*, Phys. Rev. B **63**, 134524 (2001).
- ⁹⁵ K. Kuroki, *Pairing Symmetry Competition in Organic Superconductors*, J. Phys. Soc. Jpn. **75**, 051013 (2006).
- ⁹⁶ R. Tazai, Y. Yamakawa, M. Tsuchiizu, and H. Kontani, *Prediction of pseudogap formation due to d-wave bond-order in organic superconductor κ -(BEDT-TTF) $_2$ X*, arXiv:2010.15516: to be published in Phys. Rev. Research.
- ⁹⁷ W. Ku, T. Berlijn, and C.-C. Lee, *Unfolding First-Principles Band Structures*, Phys. Rev. Lett. **104**, 216401 (2010).
- ⁹⁸ R. Tazai, Y. Yamakawa, and H. Kontani, *Emergence of Charge Loop Current in Geometrically Frustrated Hubbard Model: Functional Renormalization Group Study*, arXiv:2010.16109: to be published in Phys. Rev. B.
- ⁹⁹ D. Bohm, *Note on a Theorem of Bloch Concerning Possible Causes of Superconductivity*, Phys. Rev. **75**, 502 (1949).
- ¹⁰⁰ Y. Fuseya, M. Tsuchiizu, Y. Suzumura, and C. Bourbonnais, *Role of Interchain Hopping in the Magnetic Susceptibility of Quasi-One-Dimensional Electron Systems*, J. Phys. Soc. Jpn. **76**, 014709 (2007).
- ¹⁰¹ H. Kontani, *Anomalous transport phenomena in Fermi liquids with strong magnetic fluctuations*, Rep. Prog. Phys. **71**, 026501 (2008).
- ¹⁰² T. Moriya and K. Ueda, *Spin fluctuations and high temperature superconductivity*, Adv. Phys. **49**, 555 (2000).
- ¹⁰³ K. Yamada, *Electron Correlation in Metals*, (Cambridge University Press, Cambridge, 2004)
- ¹⁰⁴ T. Nishikawa, J. Takeda, and M. Sato, *Transport Anomalies of High-T c Oxides above Room Temperature*, J. Phys. Soc. Jpn. **63**, 1441 (1994).
- ¹⁰⁵ J. Chang, E. Blackburn, O. Ivashko, A. T. Holmes, N. B. Christensen, M. Hücker, Ruixing Liang, D. A. Bonn, W. N. Hardy, U. Rütt, M. v. Zimmermann, E. M. Forgan, S. M. Hayden, *Magnetic field controlled charge density wave coupling in underdoped YBa $_2$ Cu $_3$ O $_{6+x}$* , Nat. Comm. **7**, 11494 (2016).
- ¹⁰⁶ S. Gerberl, H. Jang, H. Nojiri, S. Matsuzawa, H. Yasumura, D. A. Bonn, R. Liang, W. N. Hardy, Z. Islam, A. Mehta, S. Song, M. Sikorski, D. Stefanescu, Y. Feng, S. A. Kivelson, T. P. Devereaux, Z.-X. Shen, C.-C. Kao, W.-S. Lee, D. Zhu, J.-S. Lee, *Three-dimensional charge density wave order in YBa $_2$ Cu $_3$ O $_{6.67}$ at high magnetic fields*, Science **350**, 949 (2015).
- ¹⁰⁷ H.-H. Kim, E. Lefrancois, K. Kummer, R. Fumagalli, N.B. Brookes, D. Betto, S. Nakata, M. Tortora, J. Porras, T. Loew, M.E. Barber, L. Braicovich, A.P. Mackenzie, C.W. Hicks, B. Keimer, M. Minola, and M. Le Tacon, *Charge Density Waves in YBa $_2$ Cu $_3$ O $_{6.67}$ Probed by Resonant X-Ray Scattering under Uniaxial Compression*, Phys. Rev. Lett. **126**, 037002 (2021).
- ¹⁰⁸ R. Tazai and H. Kontani, *Hexadecapole Fluctuation Mechanism for s-wave Heavy Fermion Superconductor CeCu $_2$ Si $_2$: Interplay between Intra- and Inter-Orbital Cooper Pairs*, J. Phys. Soc. Jpn **88**, 063701 (2019).
- ¹⁰⁹ R. Tazai and H. Kontani, *Fully gapped s-wave superconductivity enhanced by magnetic criticality in heavy-fermion systems*, Phys. Rev. B **98**, 205107 (2018).
- ¹¹⁰ R. Tazai and H. Kontani, *Multipole fluctuation theory for heavy fermion systems: Application to multipole orders in CeB $_6$* , Phys. Rev. B **100**, 241103(R) (2019). Phys. Rev. Lett. **126**, 037002 (2021).